The definitive version was published in *Science* on 12th April 2013, volume: 340, issue: 6129, pp. 183-186.
DOI: 10.1126/science.1228729
Click here to be linked to the version of record.

Speleothems reveal 500 kyr history of Siberian permafrost

Vaks, A.[1]*, Gutareva, O.S.[2], Breitenbach, S.F.M.[3], Avirmed, E.[4], Mason, A.J.[1], Thomas, A.L.[1], Osinzev, A.V.[5], Kononov, A.M.[2], & Henderson, G.M.[1]

[1]Department of Earth Sciences, University of Oxford, South Parks Road, OX1 3AN Oxford, United Kingdom

[2]Institute of Earth's Crust, Russian Academy of Sciences, Siberian Branch, 128 Lermontova Street, Irkutsk 664033, Russia

[3]Swiss Federal Institute of Technology Zurich (ETHZ), Sonneggstrasse 5, ch-8092 Zurich, Switzerland

[4] Institute of Geography, Mongolian Academy of Sciences, 210620 UlaanBaatar, Mongolia

[5]Arabica Speleological Club, Mamin-Sibiryak Street, Irkutsk 554082, Box 350, Russia

*corresponding author: Anton.Vaks@earth.ox.ac.uk; Phone: +44(0)18652-272011; Fax: +44(0)18652-72072.

Soils in permafrost regions contain twice as much carbon as the atmosphere, and permafrost has an important influence of the natural and built environment at high northern latitudes. The response of permafrost to warming climate is uncertain and occurs on timescales longer than has been assessed by direct observation. In this study, we date periods of speleothem growth in a north-south transect of caves in Siberia to reconstruct the history of permafrost in past climate states. Speleothem growth is restricted to full interglacial conditions in all studied caves. In the northernmost cave (at 60^{o}N), no growth has occurred since Marine Isotopic Stage (MIS) 11. Growth at that time indicates that global climates only slightly warmer than today are sufficient to thaw significant regions of permafrost.

Permafrost regions (in which the ground is frozen throughout the year) cover 24% of the northern-hemisphere land surface and hold ≈1700 Gt of organic carbon. When it thaws it releases CO_2 and CH_4, turning a long-term carbon sink into a source and enhancing the greenhouse effect (*1-2*). Permafrost degradation also intensifies thermo-karst development, coastline erosion and liquefaction of ground previously cemented by ice. The latter endangers infrastructure including major Siberian oil and gas facilities (*3*). An ability to predict the extent of future permafrost degradation is desirable.

Assessing the response of permafrost to changing climate is challenging. Significant warming and thawing of local permafrost conditions are seen in instrumental records during the last 20 years (*4*) but permafrost response at regional scale is slow to respond to warming and instrumental records are insufficient to capture the long-term behavior. To understand the long-term response of permafrost to climate change requires knowledge of past permafrost conditions.

Dating of organic material (*5*) or ground ice (*6*) can indicate the age of existing permafrost, but cannot reveal the longer-term history of permafrost.

In this study, we use cave carbonates (speleothems) as a tool to date past permafrost and its relationship to global climate. Vadose speleothems (stalactites, stalagmites and flowstones) form when meteoric waters (i.e. water originating from atmospheric precipitation) seep through the vadose zone into caves. Cave temperatures usually approximate the local mean annual air temperatures (MAAT), because of buffering by the surrounding rock (*7*). When cave temperatures drop below 0°C, waters freeze and speleothem growth ceases. Speleothems found in modern permafrost regions are therefore relicts from warmer periods before permafrost formed (*8-10*). Absence of water also prevents speleothem growth in arid settings, so speleothem growth episodes in modern deserts are proxies for past wet periods (*11*). Because speleothems can be robustly and precisely dated with U-Th techniques, they provide a detailed history of periods when liquid water was available, and both permafrost and desert conditions were absent.

We reconstruct the history of Siberian permafrost (and the aridity of the Gobi Desert) during the last ~500 kyr using U-Th dating of speleothems in six caves along a north-south transect in northern Asia from Eastern Siberia at 60.2°N to the Gobi Desert at 42.5°N (Fig. 1). The northernmost cave - Lenskaya Ledyanaya sits today on the boundary of continuous permafrost with MAAT substantially below 0°C (*12*). The permafrost type changes to the south-west to discontinuous, sporadic, and then to permafrost-free conditions (*13*) (Fig. 1). Annual precipitation in this Siberian region is 400-600 mm/y falling mainly during summer. To the south, in the Gobi, MAAT ranges from +2°C to +8°C and little precipitation falls (200-80 mm/y) (*14*).

Speleothem thickness provides an indication of long-term liquid-water availability along the transect. Only 8 cm of growth is seen in the northernmost cave, increasing to ~70 cm in the caves of southern Siberia and decreasing again to less than 30 cm in the Gobi. As expected, southern Siberia is more suitable for speleothem growth than the cold north or the dry south. All recovered speleothems show a texture of calcium-carbonate layers alternating with growth hiatuses (see Supporting Online Material; SOM).

Thirty-six speleothems were collected from the caves and 111 U-Th ages conducted (Fig 2A). In each speleothem, at least one sample was taken from the outermost layer and from each section of growth (i.e. between hiatuses) inward, until the limits of the U-Th chronology were reached (~500 ka) to assess all periods of growth. A full description of the samples, and their sub-sampling and dating is given in the SOM.

The youngest speleothem growth in the region of modern continuous permafrost (i.e. at 60°N) occurred during interglacial MIS-11, contrasting with the centre of the transect where speleothems grew during all interglacials (Fig. 2A, B). Age ranges in southern Siberia also demonstrate that the duration of speleothem deposition in MIS-11 was longer than during subsequent interglacials. These observations indicate that permafrost thawing during MIS-11 was more extensive than at any other point during the last 450 kyr and extended northward of 60°N, significantly further north than the present limit of continuous permafrost. Some similar thawing may also have occurred at MIS-13 in this most northerly cave. The absence of any observed speleothem growth since MIS 11 in the northerly Lenskaya Ledyanaya cave (despite dating outer edges of 7 speleothems), suggests the permanent presence of permafrost at this latitude since the end of MIS-11. Speleothem growth in this cave occurred in early MIS-11, ruling out the possibility that the unusual length of MIS-11 caused the permafrost thawing.

MIS-11 was also characterized by wetter conditions in the Mongolian Gobi Desert, as shown by two ages from Shar-Khana Cave speleothems (Fig. 2A), which contrast with the absence of growth during subsequent interglacials. The existence of a humid event in the Gobi during early MIS-11 is supported by mollusk assemblages from Chinese Loess Plateau (*15*), and by the dominance of input into Lake Baikal via the Selenga River during MIS-11 (*16*).

The degradation of permafrost at 60°N during MIS-11 allows an assessment of the warming required globally to cause such extensive change in the permafrost boundary. There is significant evidence that MIS-11 was the warmest of recent interglacials, including the presence of boreal forest on South Greenland at that time (*17*), the absence of ice-rafted debris in the North Atlantic (*18*), increased sea levels (*19*), and higher sea-surface temperatures (SST) in the tropical Pacific (*20-22*). Mg/Ca reconstructions (*21-22*) indicate that SST of the Pacific Warm Pool (PWP) reached >30°C in early MIS-11, compared to 29.5°C in MIS-5.5 and ~28.5°C during the pre-industrial Late Holocene (Fig. 2D). This tropical heat was transported poleward (*23*) and there is evidence of unusual warmth in Siberia during MIS-11, evidenced by the high fraction of biogenic silica in the sediments of Lake Baikal (*24*) (Fig. 2C) and high spruce pollen content in Lake El'gygytgyn, suggesting local temperatures 4-5°C above present (*25*). When PWP temperatures reach 30°C this appears to cause more pronounced warming of northern continents, and lead to significant northward migration of the permafrost boundary.

Periods of Siberian speleothem growth since MIS-11 suggest a close link between greenhouse warming/global temperatures and permafrost extent. After a brief post MIS-11 hiatus in growth (from 370 to 355 ka), coinciding with a minimum in atmospheric CO_2 and in PWP SST during MIS-10 (Fig. 2D, F), significant thicknesses of speleothem grew in Southern Siberia during MIS-9 as greenhouse gases returned to higher values. Speleothems also grew actively during MIS-5.5

and the Holocene (>5 cm) when CO_2 levels were high. In contrast, growth during MIS-7, a period of lower CO_2 and cooler global conditions, is minimal (maximum 1.5 cm in any studied cave) and no growth is observed during MIS-5.4 to 5.1. Conditions during MIS-7 were at the very limit for growth in southern Siberia: speleothems grew during MIS-7.3 and 7.1 in Okhotnichya Cave (52^{o}N) but only during MIS-7.1 just to the north at Botovskaya Cave (55^{o}N). No growth occurred during MIS-7.5 at either cave despite higher concentrations of CO_2 and CH_4 than later in MIS-7 (*26-27*) and high PWP SST (Fig 2D-F) (*21-22*). Lake Baikal biogenic silica (*24*) and the percentage of arboreal pollen in Lake El'gygytgyn sediments (*28*) are also lower during MIS-7.5 than during MIS-7.3 and 7.1. Lower local summer insolation during MIS-7.5 (Fig 2G) (*29*) suggests a role for local insolation in overprinting a Siberian climate dominantly controlled by global greenhouse gas levels.

U-Th dating of Siberian speleothem growth during recent interglacials allows detailed comparison of permafrost history with other aspects of the global climate system (Fig 3). During MIS-5.5, speleothems started growing between 128.7 and 127.3 ka, and ended between 119.2 and 118.1 ka (determined from Bayesian analysis of U-Th data using OxCal-4.1; see SOM for details). The permafrost thawing initiated when insolation was close to its maximum and greenhouse gases had just reached maximum values. Holocene permafrost degradation at our sites lags maximum insolation and greenhouse gas concentrations slightly, and starts between 10.0 and 9.8 ka. This lag may be due to the time required for permafrost to thaw at the slightly lower insolation and CO_2 levels of the Holocene (relative to MIS-5.5).

Overall, dated periods of speleothem growth allow an assessment of the relationship between global temperature and permafrost extent. PWP SST was 0.5-1.0°C higher during MIS-5.5 and ≈1.5°C higher during early MIS-11 relative to the pre-industrial Late Holocene (Fig. 2D) (*21-*

22). Using PWP SST as a surrogate for global temperature (*21*) suggests that increase in global temperatures by 0.5-1.0°C will degrade only non-continuous permafrost in southern Siberia with the Gobi Desert remaining arid. Warming of ≈1.5°C (i.e. as in MIS-11) may cause a substantial thaw of continuous permafrost as far north as 60°N, and create wetter conditions in the Gobi Desert. Such warming is therefore expected to dramatically change the environment of continental Asia, and can potentially lead to substantial release of carbon trapped in the permafrost into the atmosphere.

Acknowledgments

This article is dedicated to the memory of Prof. Y. Trzhcinski, who during the last months of his life made a big effort to establish the cooperation between University of Oxford and Institute of Earth's Crust (IEC) in Irkutsk. Thanks to D. Sokolnikov and other 'Arabica' members, E. Kozireva (IEC), V. Alexioglo and V. Balaev from Lensk for their help during the fieldwork in Siberia, Mongolian Speleological Society for their help with the fieldwork in Mongolia; to J. Fritz and L. Zehnder (ETH Zurich) for drawing Fig. 1 and for assistance with XRD analyses respectively; to C. Day, V. Ersek, P. Holdship, O. Green, S. Wyatt, Y. Nakajima, P. Pousada Solino and others from University of Oxford for the help with the laboratory work, administration issues and fruitful discussions. This work was funded by NERC Fellowship NE/G013829/1, Royal Society grant JP080831 and Russian Foundation for Basic Research joint grant 09-05-92605 KO_a.

Figure captions:

Figure 1: Map showing the extent of permafrost types in eastern Siberia, the Gobi Desert, and the location of studied caves (black circles). Permafrost data is taken from Brown et al. (2001) (*30*).

Figure 2: (A) Distribution of speleothem U-Th ages (±2σ) in time and space (*n* – total number of U-Th age determinations per cave, including those beyond the U-Th range) with grey bars signifying periods of growth in Okhotnichya and Botovskaya caves. (B) Benthic $\delta^{18}O$ stack (*31*) with MIS numbers. (C) Concentration of biogenic silica in Lake Baikal sediments (%) (*24*). (D) Pacific Warm Pool Mg/Ca SST, with the pre-industrial Late Holocene SST shown by red horizontal fragmented line (*21-22*). (E, F) CH_4 and CO_2 records of EPICA Dome C respectively (*26-27*). (G) Summer insolation at 55°N (*29*). Speleothems with ages exceeding 500 ka (within ±2σ range) are not shown, but accounted for in *n*. Two samples SLL9-2-A+B and SOP-32-B are not included because they reflect a mixture of material from different layers; please refer to the Supplementary Table 1.

Figure 3: Siberian speleothem growth periods during Holocene and MIS-5.5 (A) with grey bars indicating periods of growth. Compared with East-Asian Monsoon record from Hulu and Sanbao caves (B) (*32*), GICC05 $\delta^{18}O$ (C) (*33-34*), CH_4 (D) and CO_2 (E) records of EPICA Dome C (*26-27*), and 55°N summer insolation (F) (*29*).

References and Notes:

1. G. Grosse, V. Romanovsky, *EOS* **92**, 73 (2011).
2. E. A. G. Schuur *et al.*, *BioScience* **58**, 701 (2008).
3. O. Anisimov, S. Reneva, *AMBIO: A Journal of the Human Environment* **35**, 169 (2006).
4. V. E. Romanovsky, S. L. Smith, H. H. Christiansen, *Permafrost and Periglacial Processes* **21**, 106 (2010).
5. Y. K. Vasil'chuk, J.-C. Kim, A. C. Vasil'chuk, *Nuclear Instruments and Methods in Physics Research Section B: Beam Interactions with Materials and Atoms* **223-224**, 650 (2004).
6. D. A. Gilichinsky *et al.*, *Quaternary Science Reviews* **26**, 1547 (2007).
7. H. P. Schwarcz, in *Handbook of Environmental Isotope Geochemistry*, P. Fritz, J. C. Fontes, Eds. (Elsevier, Amsterdam, 1986), vol. 2, pp. 271-300.
8. R. A. Cliff, C. Spötl, A. Mangini, *Quaternary Geochronology* **5**, 452 (2010).
9. B. Lauriol, D. C. Ford, J. Cinq-Mars, W. A. Morris, *Canadian Journal of Earth Sciences* **34**, 902 (1997).
10. S. E. Lauritzen, *Quaternary Research* **43**, 133 (1995).

11. A. Vaks, M. Bar-Matthews, A. Matthews, A. Ayalon, A. Frumkin, *Quaternary Science Reviews* **29**, 2647 (2010).
12. Philip's, Ed., *Modern School Atlas, 95-th edition*, (Philip's, a division of Octopus Publishing Group Limited, London, 2007).
13. A. Jones *et al.*, Eds., *Soil Atlas of the Northern Circumpolar Region*, (European Commission, Publication Office of the European Union, Luxembourg, 2010), pp. 144.
14. D. Dorjotov, N. Orshikh, T. Oyunchimeg, *Geographic Atlas of Mongolian Republic (in Mongolian)*. (Mongolian Institute of Geodesy and Cartography Ulaanbaatar, Mongolia, 2004), pp. 64.
15. N. Wu *et al.*, *Quaternary Science Reviews* **26**, 1884 (2007).
16. A. W. Mackay *et al.*, *Journal of Quaternary Science* **23**, 365 (2008).
17. A. de Vernal, C. Hillaire-Marcel, *Science* **320**, 1622 (2008).
18. J. F. McManus, D. W. Oppo, J. L. Cullen, *Science* **283**, 971 (1999).
19. M. E. Raymo, J. X. Mitrovica, *Nature* **483**, 453 (2012).
20. L. Ortlieb, A. Diaz, N. Guzman, *Quaternary Science Reviews* **15**, 857 (1996).
21. J. Hansen *et al.*, *Proceedings of the National Academy of Sciences* **103**, 14288 (2006).
22. M. Medina-Elizalde, D. W. Lea, *Science* **310**, 1009 (2005).
23. A. J. Dickson *et al.*, *Nature Geosci* **2**, 428 (2009).
24. A. A. Prokopenko *et al.*, *Quaternary Research* **55**, 123 (2001).
25. M. Melles *et al.*, *Science* **337**, 315 (2012).
26. L. Loulergue *et al.*, *Nature* **453**, 383 (2008).
27. D. Luthi *et al.*, *Nature* **453**, 379 (2008).
28. N. R. Nowaczyk *et al.*, *Geophysical Journal International* **150**, 109 (2002).
29. J. Laskar *et al.*, *Astronomy and Astrophysics* **428**, 261 (2004).
30. J. Brown, J. O. J. Ferrians, J. A. Heginbottom, E. S. Melnikov. (National Snow and Ice Data Center/World Data Center for Glaciology. Digital media., Boulder, CO, 2001).
31. L. E. Lisiecki, M. E. Raymo, *Paleoceanography* **20**, (2005).
32. Y. Wang *et al.*, *Nature* **451**, 1090 (2008).
33. S. O. Rasmussen *et al.*, *J. Geophys. Res.* **111**, D06102 (2006).
34. See references 16 to 19 in the supplementary materials.

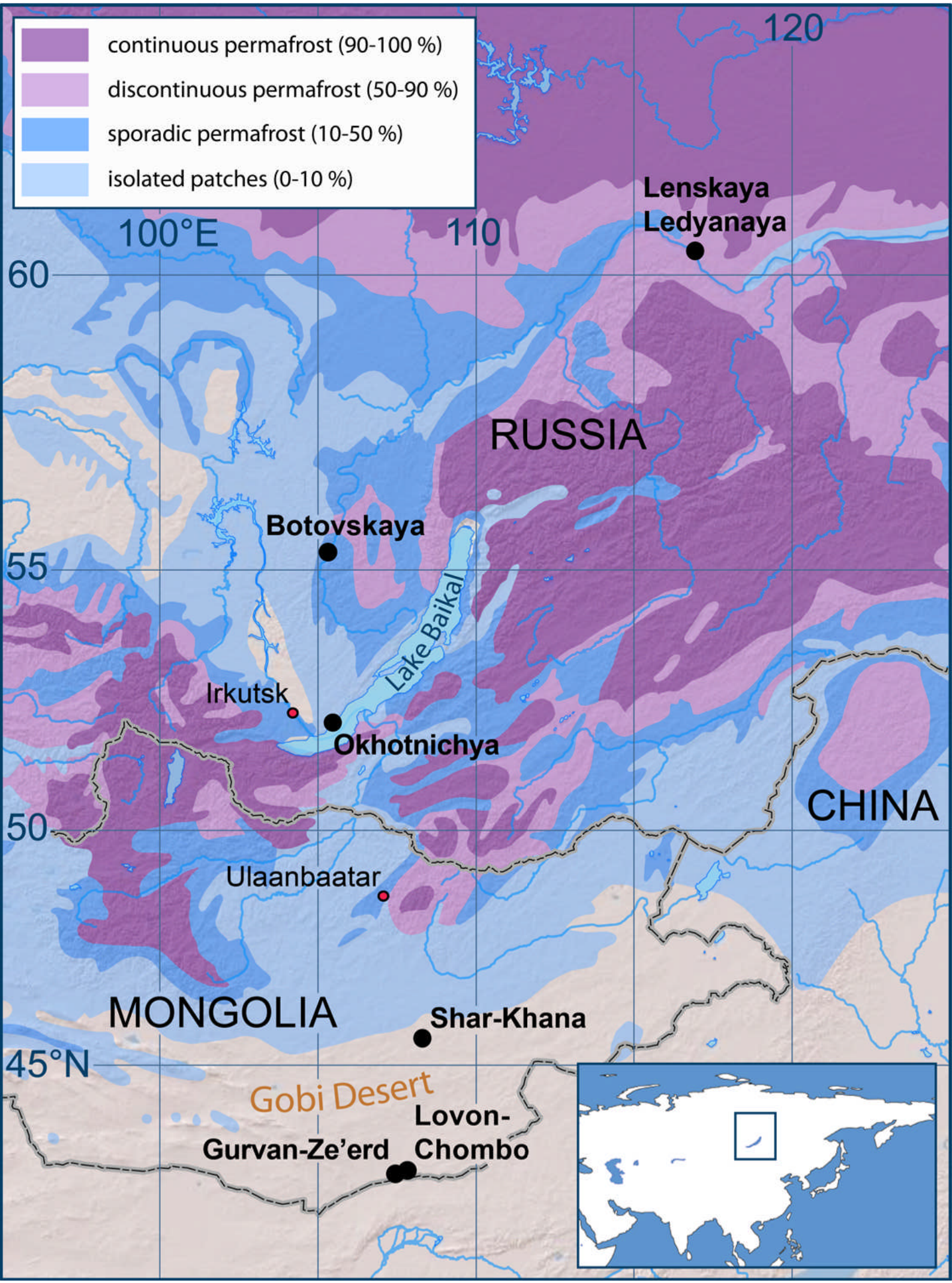
continuous permafrost (90-100 %)
discontinuous permafrost (50-90 %)
sporadic permafrost (10-50 %)
isolated patches (0-10 %)
120
100°E
110
60
55
50
45°N
Lenskaya
Ledyanaya
RUSSIA
Botovskaya
Lake Baikal
Irkutsk
Okhotnichya
CHINA
Ulaanbaatar
MONGOLIA
Shar-Khana
Gobi Desert
Lovon-
Gurvan-Ze'erd
Chombo

Figure 2 :

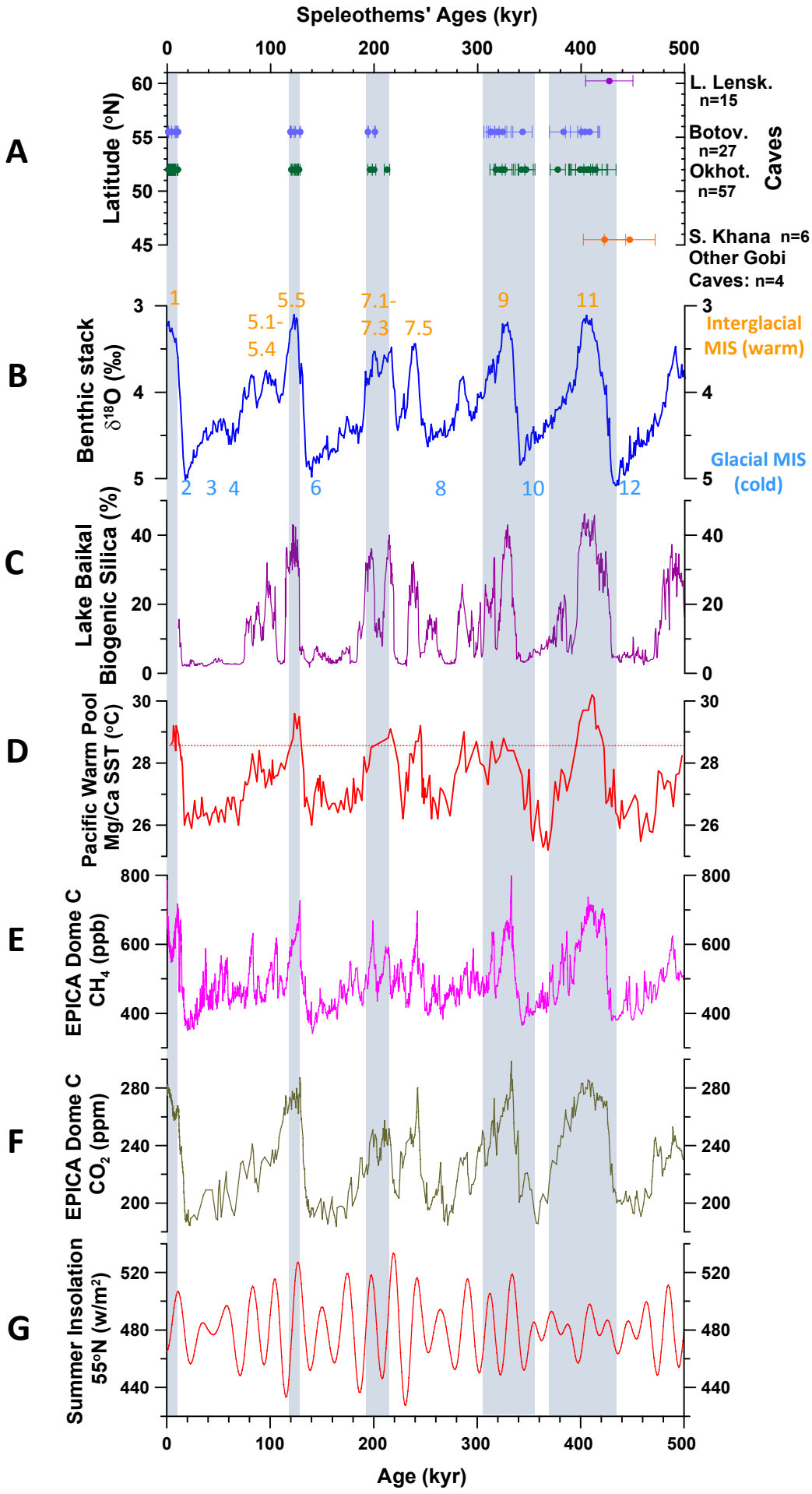
Speleothems' Ages (kyr)
0
100
200
300
400
500
A
Latitude (°N)
60
55
50
45
L. Lensk. n=15
Botov. n=27
Okhot. n=57
Caves
S. Khana n=6
Other Gobi Caves: n=4
B
Benthic stack δ18O (‰)
3
4
5
1
5.1-5.4
5.5
7.1-7.3
7.5
9
11
2
3
4
6
8
10
12
Interglacial MIS (warm)
Glacial MIS (cold)
C
Lake Baikal Biogenic Silica (%)
40
20
0
D
Pacific Warm Pool Mg/Ca SST (°C)
30
28
26
E
EPICA Dome C CH4 (ppb)
800
600
400
F
EPICA Dome C CO2 (ppm)
280
240
200
G
Summer Insolation 55°N (w/m²)
520
480
440
Age (kyr)

Figure 3:

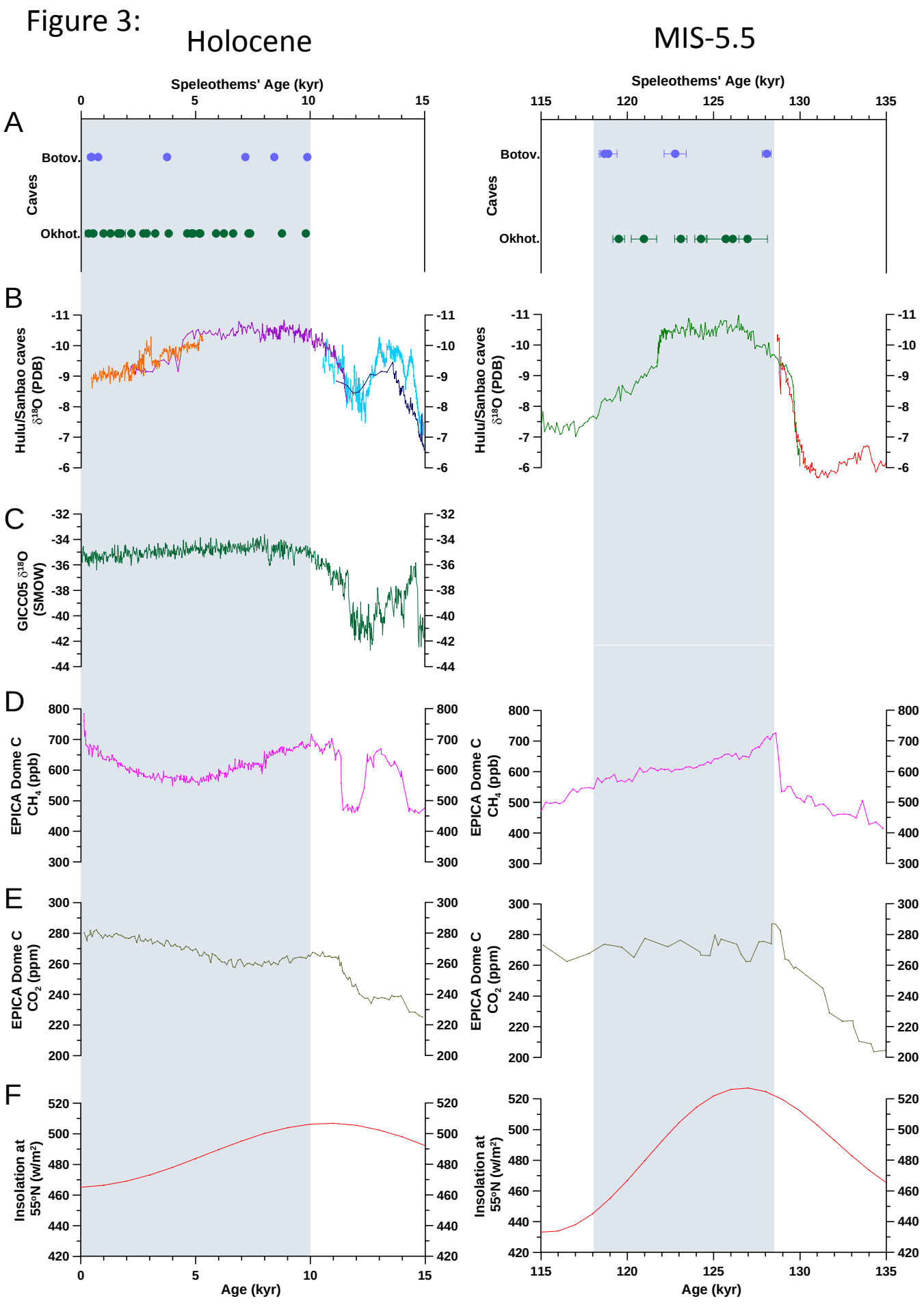
Holocene
MIS-5.5
Speleothems' Age (kyr)
A
Botov.
Okhot.
Caves
B
Hulu/Sanbao caves
δ18O (PDB)
C
GICC05 δ18O
(SMOW)
D
EPICA Dome C
CH4 (ppb)
E
EPICA Dome C
CO2 (ppm)
F
Insolation at
55°N (w/m²)
Age (kyr)

Supporting online material

Table of contents:

Description of the caves:

Ledyanaya Lenskaya Cave:

Located at 60°22'16"N-116°56'47"E, 116 km E-S-E from the town of Lensk, 180 m above sea level, on the north-eastern bank of the Lena River in a cliff ~50 m above the river. The vegetation is sub-boreal taiga forest with precipitation of ~400 mm/y, and monthly mean air temperatures range from 18°C in July to -32°C in January (*1*). The cave is located in Cambrian limestones and marls; its length is ~130 m, consisting of one main passage 90 m long going from the entrance in a N-NE direction and ascending by ~10°, ending with a large hall partially filled with massive ice. The ice is many meters thick and it is unknown if there are any speleothems buried under it. A few narrow moderately ascending corridors split from the main passage in E-NE direction and end in small chambers in which inactive vadose speleothems are found (Suppl. Fig. 1). The depth of the chamber containing speleothems is 15-20 m, and the depth of the large hall with ice is ~60 m below the surface.

According to the permafrost map of Ershov (1991) (*2*) the cave is located under "mainly continuous permafrost" up to 50 m thick, that may contain 3-5% of through and not through taliks (permafrost type 18 on the map; taliks - small patches of unfrozen ground). The air temperature in the lower part of the main corridor is -3.5°C (in March 2010, with outside temperature -19°C) increasing in the upper parts of the cave to 0.0°C - +0.4°C in the hall with the massive ice, and to +0.8°C in the chamber with speleothems. Although the temperatures there are slightly above zero, no water seepage or speleothem growth was found in August 2009 or March 2010, showing that the rock above the cave is completely frozen with no presence of through taliks above the cave. The ice in the uppermost part of the cave is forming from condensation and freezing of outside atmospheric vapour. The formation of this ice is most intense in summer, when the air entering the cave is warm and humid. In winter the amount of ice decreases because of sublimation of the vapour from the cave into the cold dry air outside. According to Ford and Williams (1989), p. 351 (*3*), formation of ice in the uppermost and warmest part of caves shows that the cooling that creates the ice occurs when warm and moist air from outside the cave comes in contact with frozen rock inside the cave, so the ice in Ledyanaya Lenskaya Cave indicates the presence of permafrost. In the ice hall remnants of a fireplace lit by modern local visitors was found on the ice. The later could also contribute to the relatively high modern cave temperatures. Historical evidence from the 18th century reports a much colder air temperature of -10.4°C (-8.3°R, mercury thermometer, Reaumur Scale) in the ice hall during summer time, when the outside temperature was +22°C (+17.5°R) (*4*), showing that at the end of the Little Ice Age the cave's temperatures were much lower than today. Formation of speleothems in Ledyanaya Lenskaya Cave in the past presents evidence of permafrost degradation from "mainly continuous" type (18 at Suppl. Fig. 2) to one of the discontinuous types (15-17 at Suppl. Fig. 2) at least.

Supplementary Figure 1: Lenskaya Ledyanaya Cave, map and cross-section.

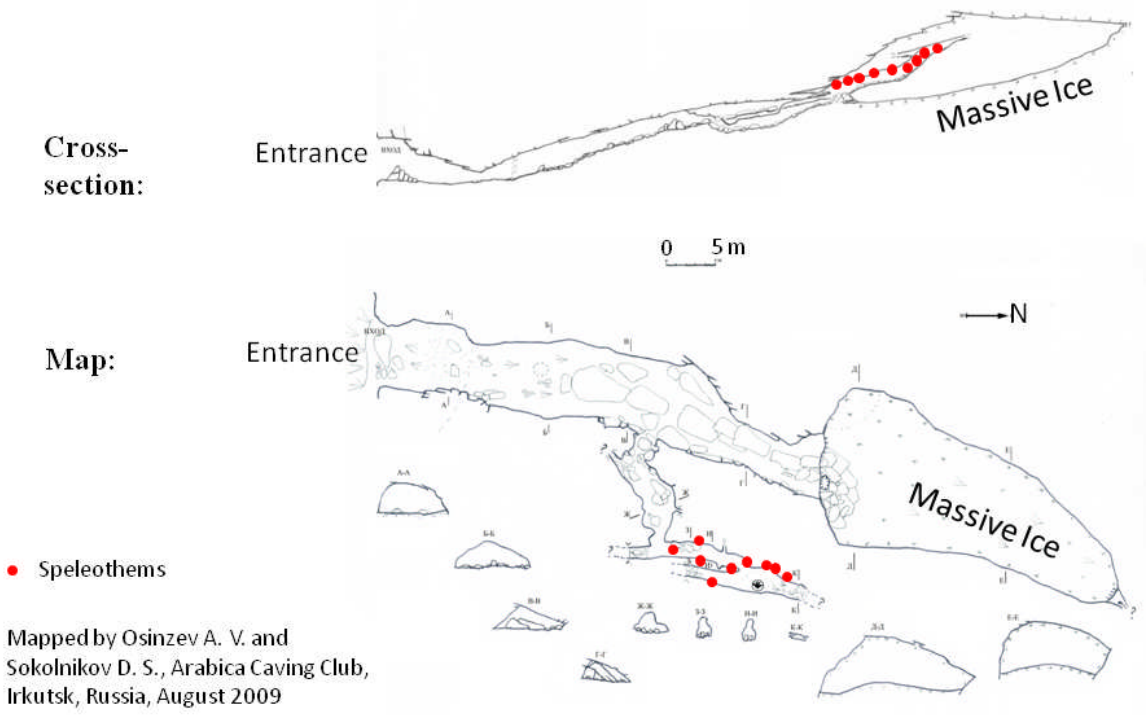

Supplementary Figure 2: Permafrost settings in which Lenskaya Ledyanaya Cave (red circle) is located (*2*).

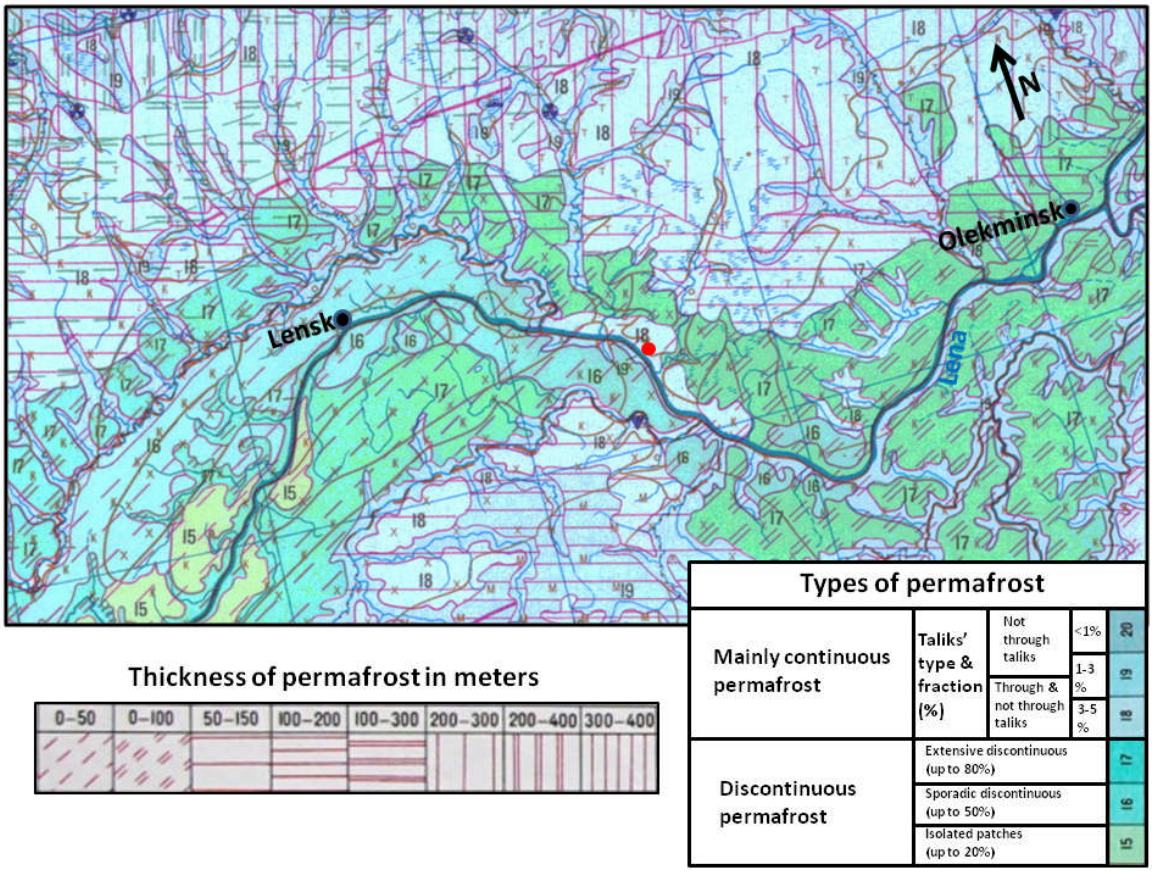

Botovskaya Cave:

Located at 55°17'59"N-105°19'46"E, 58 km N-NE from the town of Zhigalovo, 750 m above sea level, at the head of a small valley NE of the Boti River. The latter joins the Lena River 8.6 km SE from the cave. The vegetation is sub-boreal taiga forest with precipitation of ~400 mm/y, and monthly mean air temperatures ranging from 18°C in July to -28°C in January (*1*). The cave is located in Ordovician limestones and sandstones. This is one of the longest karstic cave systems in Russia, reaching a total length of more than 64 km. The cave is a horizontal maze of thousands of passages developed along the crisscross system of tectonic fissures (Suppl. Fig. 3). The depth of the cave is 40-130 m below the surface and the cave air temperatures vary from ≤0°C in the cold zones to 1.6-1.9°C in its warmest parts (Suppl. Fig. 4). The temperatures in the cave and outside were monitored between February 2010 and February 2011. Mean annual air temperature outside the cave is -2.8°C, varying between summer and winter extremes from +35°C to -40°C. In places where temperature loggers were deployed the temperatures were found to be constant throughout the year, but higher than the annual mean by 4.4-4.7°C (Suppl. Fig. 4). The cave ceiling is relatively thick, whereas the permafrost thickness in this area is less than 100 m (*2*). It is therefore possible that permafrost layer prevents water from entering many parts of the cave, whereas the cave below remains warmer than 0°C. The only area where water seepage occurs and vadose speleothems grow today is the eastern part of the cave (Suppl. Fig. 3), located under a small depression at the surface. This depression allows formation of an intermittent stream that concentrates rain/snowmelt water to seep into the cave, probably causing an absence of permafrost in this local area. The majority of the studied speleothem samples were collected in this eastern part of the cave. In order not to damage the cave's natural beauty we collected only small amounts of inconspicuous stalagmite material for the study. The western part of the cave is dry (although non-active old speleothems are found there too) and some passages there are clogged with massive ice with ≤0°C temperatures, showing that the cave is located in discontinuous permafrost.

Supplementary Figure 3: Map of Botovskaya Cave with locations of speleothems and temperature loggers.

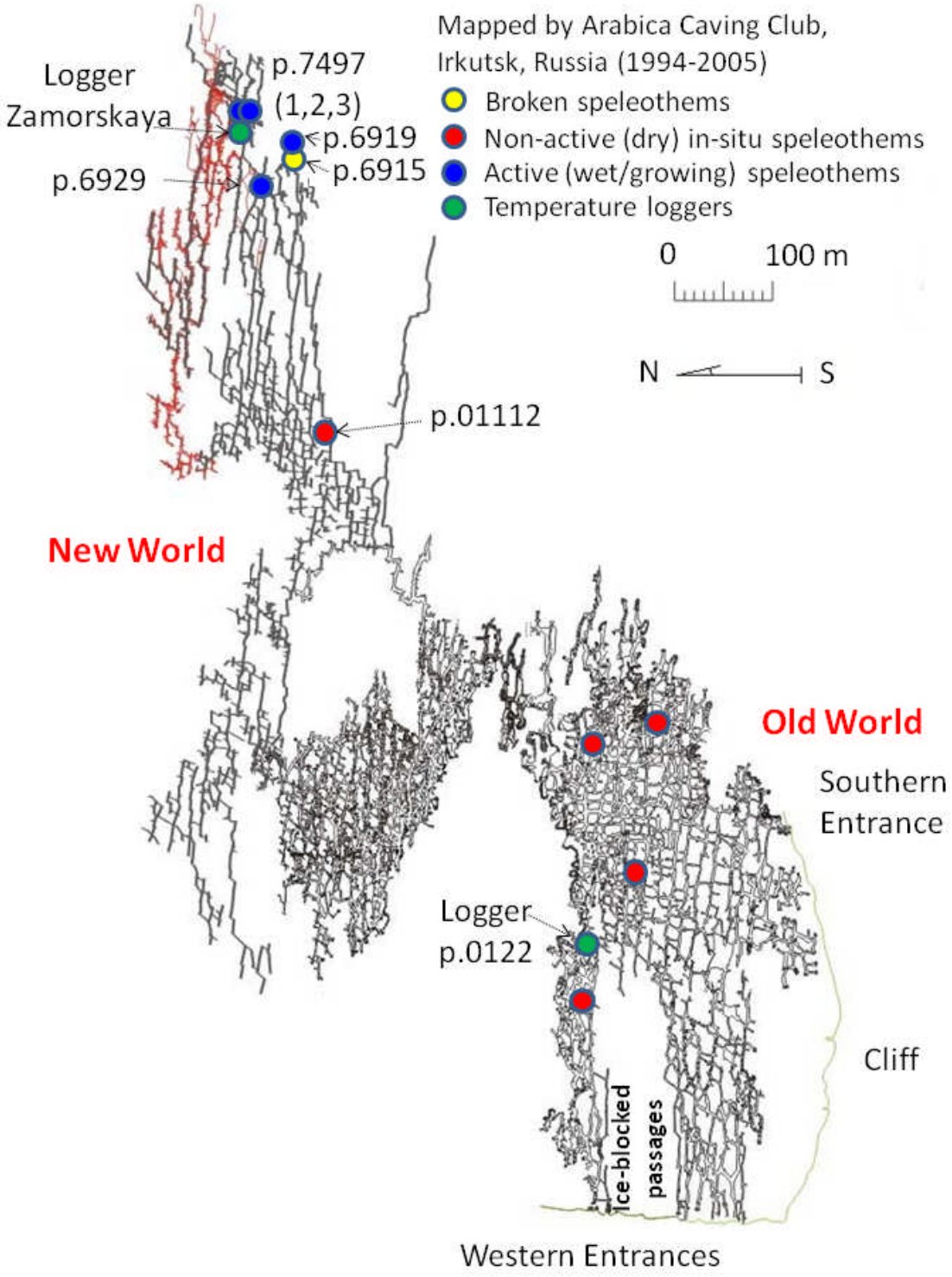

Supplementary Figure 4: Botovskaya Cave temperature (T) monitoring 2010-2011.

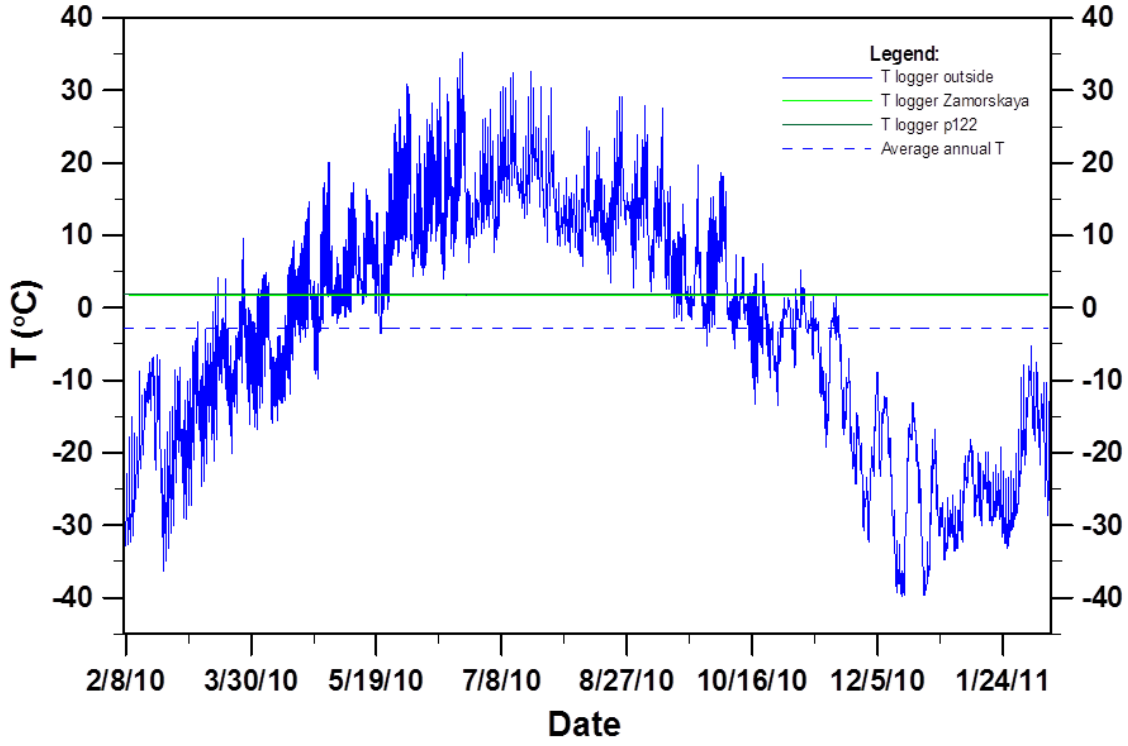

Okhotnichya Cave:

Located at 52°07'41"N-105°29'11"E, the Okhotnichya Cave is 700 m above sea level, 83 km E-SE from the city of Irkutsk, 11 km NE from the village of Bolshoe-Goloustnoe and 4.6 NW from the shore of Lake Baikal. The vegetation is mixed deciduous and conifer forest with precipitation of ~400 mm/y, and monthly mean air temperatures range from 16°C in July to -16°C in January (*5*). The cave is located in Cambrian stromatolite limestones with basaltic dykes in places. The cave has one main large entrance hall steeply descending from the entrance, and then splitting into several systems of passages oriented preferably in a NNE-SSW direction (Suppl. Fig. 5). The total length of the cave's passages is ~5700 m, and the average depth of the cave's passages is 20-30 m below the surface. Water seepage and speleothem growth can be found everywhere in the cave. Temperatures inside and outside the cave were monitored from September 2008 to November 2011 and the three-year mean air temperature outside the cave is -0.2°C, varying between the extremes of +34°C and -38°C (Suppl. Fig. 6). Cave air temperature is constant in the deep parts of the cave: 1.2°C where samples SOP-3, 5 were taken (temperature logger pk-956, Suppl. Figs. 5, 6) and 1.4°C near samples SOP-11-20 (temperature loggers Rp-7, pk-371, Suppl. Figs. 5, 6). The central part of the cave from which samples SOP-1, 2, and 25 were taken, traps cold air from the entrance during winter and the temperature there varies between 0.3°C in summer and -1.3°C in winter (temperature logger in "ikaite zone", Suppl. Figs. 5, 6). Variable small amounts of ice are found in the latter location most of the year. Slightly closer to the entrance scattered ikaite (cryogenic carbonate) crystals can be found on the floor and on fallen

boulders, presenting evidence for the existence of a large body of cave ice in the past (*6*). Water seepage is found everywhere in the cave, which indicates that the rock above the cave is mainly permafrost-free, or that isolated patches of permafrost are small in size.

Supplementary Figure 5: Map of Okhotnichya Cave with locations of speleothem samples and temperature loggers.

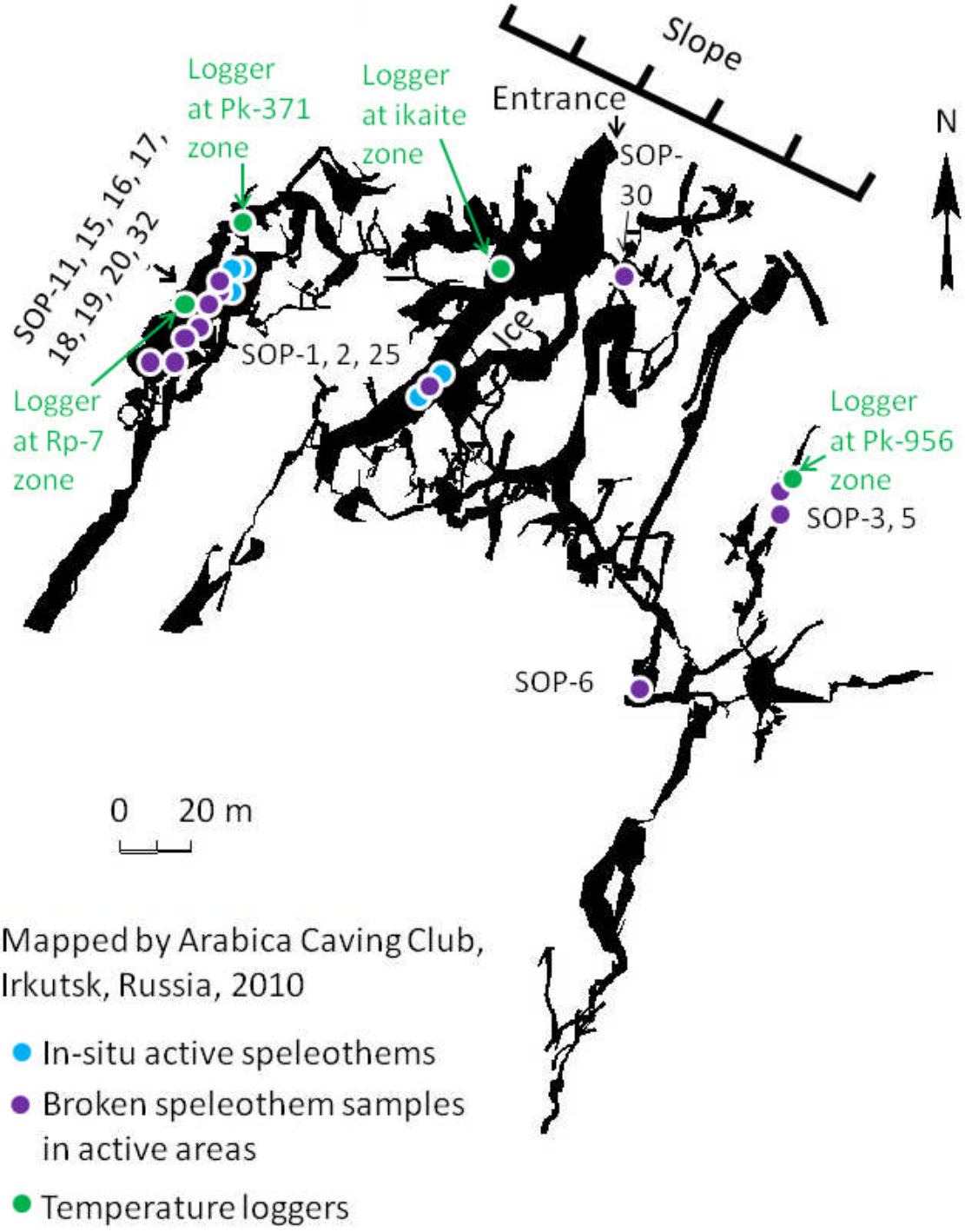

Supplementary Figure 6: Monitoring of Okhotnichya Cave Temperatures (T), 2008-2011. Average multi-annual T (fragmented blue line) is calculated between 03/09/2008 and 03/09/2011.

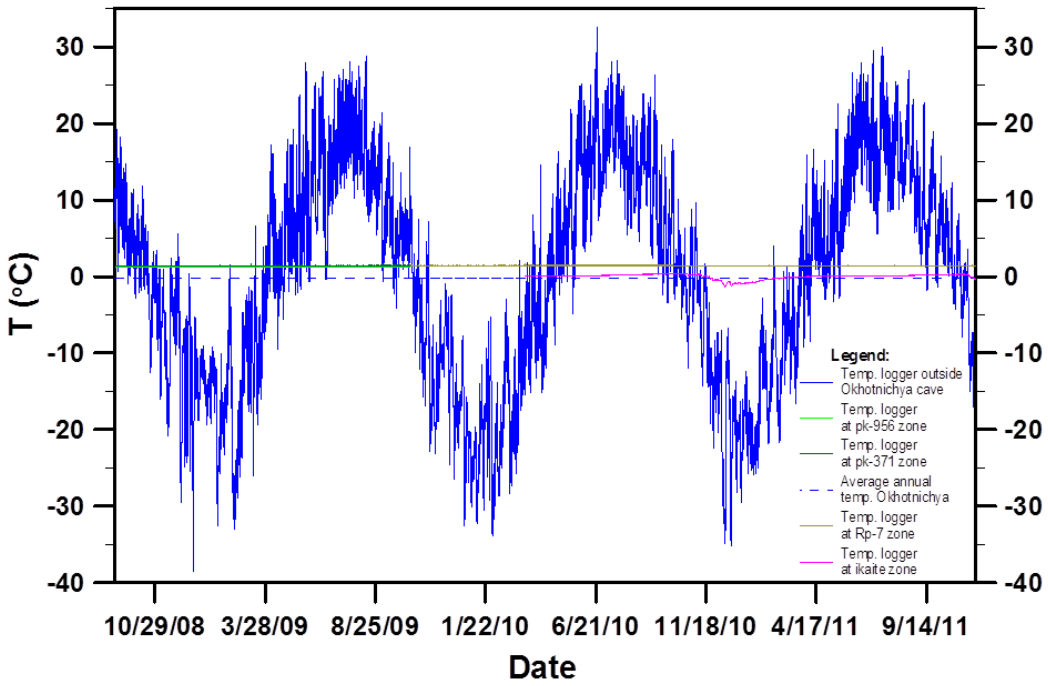

To minimize damage to the environment of the Okhotnichya Cave most samples taken were already broken (though with their initial attachment position still identified). When sampling of in-situ active speleothems was necessary, we collected hidden speleothems. In one case where this was not possible, we replaced the stalagmite (SOP-20) with a ceramic replica (Suppl. Fig. 7) to give the impression that no sample was removed.

Supplementary Figure 7: Construction of a ceramic replica stalagmite to replace a removed sample. A drip logger was also placed inside the replica. Work performed by D. Sokolnikov (top) and A. Osinzev (bottom right). The stalagmite replica was later painted in brown to make it the same colour as the surroundings.

Temperature monitoring inside/outside the Siberian caves

Hobo UA Pendant Temp Loggers were deployed in Ledyanaya Lenskaya, Botovskaya and Okhotnichya caves to monitor the cave air temperatures in places where speleothems were taken. Loggers were also placed outside the caves in the shadowy northern side of tree trunks, 2 m above the ground, to monitor the temperatures outside the caves. The logger's uncertainty is 0.47°C. The temperature data from Botovskaya and Okhotnichya caves is presented in Suppl. Figs. 4 and 6.

Shar-Khana Cave:

The cave is located at 45°35'23.1"N-108°19'18.8"E, in the Central Gobi Desert in Mongolia, 1200 m above sea level and 85 km south of the town of Choir. The vegetation is semi-desert sparse shrubs and grasses with precipitation of 130-150 mm/y, and monthly mean temperatures ranging from 22°C in July to -18°C in January (*7*). The cave is located in limestones and marbles of Upper Proterozoic, its depth varies between 13 and 25 m, with a length of 178.2 m. The cave is an underground paleo-stream channel going from ESE to WNW (125°) (Suppl. Fig. 8A) and sandy and gravel sediments washed in from the surface cover the floor. Several shafts ascend upward from the main channel and speleothems are mainly found at or beneath these shafts. The speleothems are of two types: vadose corallites and flowstone/phreatic overgrowth. The cave is completely dry, no water seepage/growing speleothems were observed. The cave air temperature is ~4°C.

Gurvan Ze'erd Cave:

The cave is located at 42°30'15.7"N-107°27'00.1"E, in the Southern Gobi Desert in Mongolia, 1075 m above sea level, 79 km SSE of the town of Khanbogd and 5 km north of the Mongolian-Chinese border. The monthly mean temperatures range from 26°C in July to -12°C in January (*7*) and the vegetation is desert sparse shrubs and grasses. Although literature reports a precipitation of 50-60 mm/y in this region (*7*), the vegetation density is similar to the Central Gobi, indicating that the real precipitation amounts may be higher. The cave is located in red limestones of Lower-Middle Proterozoic, and is ~50 m long, 30-40 m wide and 5-30 m below the surface (Suppl. Fig. 8B). The cave is composed of several round halls together with phreatic dissolution domes on the ceiling above. One of these domes was truncated by erosion forming the cave's entrance located on the NW slope of the mountain. The speleothems in the cave are mainly phreatic overgrowths covering the walls. Several stalagmite-like formations can be found on the floor, the largest is located on a rock-fall and reaching 30 cm high (Suppl. Fig. 13). The top of this speleothem was broken lying nearby and was taken, as well as two cores taken by the drilling the tops of two small stalagmite-like formations. The form of the layers in these speleothems put their vadose origin in doubt and makes their phreatic origin more likely. The cave temperature is 9.0°C. A significant part of the cave's sediments is bat guano. This guano burned at some time in the past "cooking" the outer layers of the most of the speleothems.

Lovon Chombo Cave:

The cave is located at 42°35'18.4"N-107°49'32.0"E, in the Southern Gobi Desert in Mongolia, 1195 m above sea level, 84 km SE of the town of Khanbogd and 19 km north of the Mongolian-Chinese border. The vegetation and the climate are similar to that of the Gurvan-Ze'erd cave area. The cave is located in brown limestones of Lower-Middle Proterozoic, it is ~49.5 m long, 10-20 m below the surface and composed of two halls as shown on Suppl. Fig. 8C. The floor of the larger hall covered by thick (1 m) red clay sediments and the walls of the cave are covered by phreatic overgrowth speleothems 5-15 cm thick (Suppl. Fig. 14). One broken piece of this overgrowth was sampled. In the smaller hall these phreatic speleothems have marks of past groundwater levels. The temperature in the cave is 8.8°C.

Supplementary Figure 8: Maps and cross-sections of Mongolian Caves (*8*).

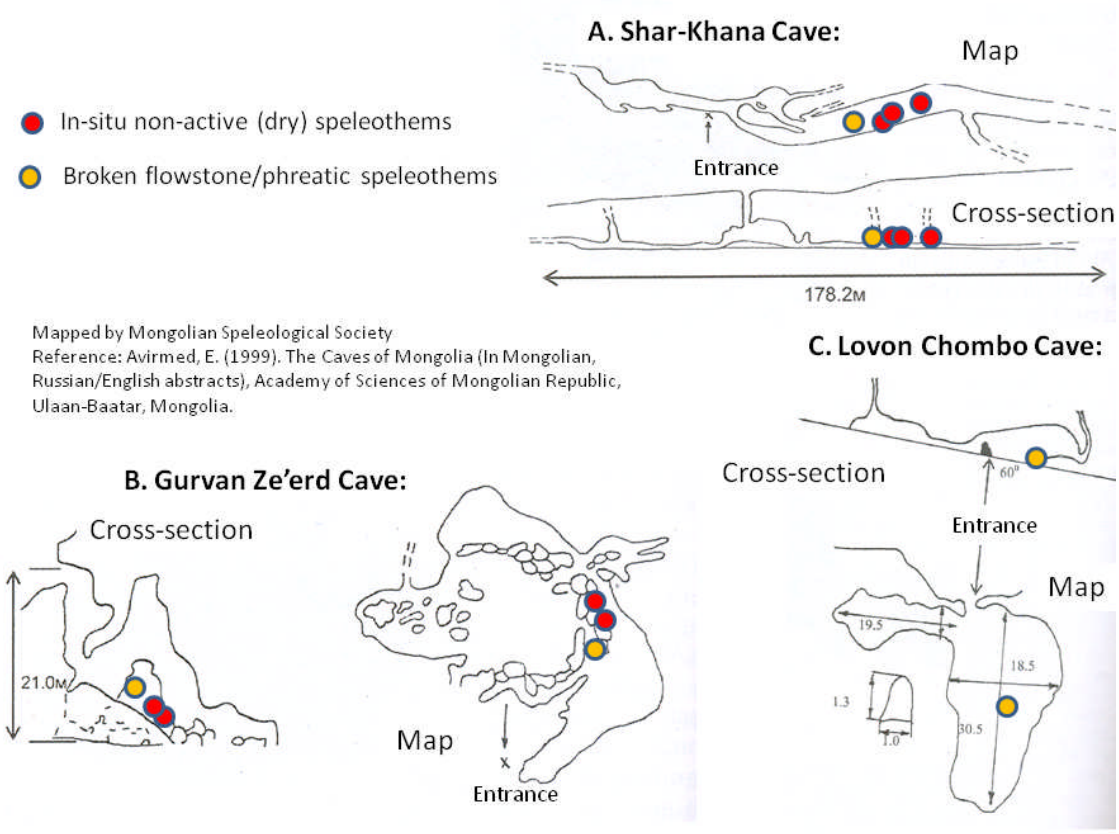

Speleothem thickness and petrography:

In the northernmost Ledyanaya Lenskaya Cave the maximum speleothem thickness (from the bedrock to the uppermost horizon) is ~8 cm. Speleothems consist of four to seven calcite horizons, each composed of brown or grey columnar calcite crystals, which are usually clean from detrital material. These calcite horizons are separated by whitish or beige thin layers of

microcrystalline calcite (<2 mm thick), sometimes containing pieces of marl and limestone host rock. The latter layers represent breaks in speleothem growth (hiatuses) with pieces of broken host rock that fell from the cave ceiling, remaining on the ancient speleothem surface (Suppl. Fig. 9).

In Botovskaya Cave, active speleothems are found in the eastern part of the cave. The western part of the cave is generally dry with no active speleothems. Maximal thickness of the speleothems in the cave is ~60 cm, showing that, compared to Ledyanaya Lenskaya Cave, the humid and less cold climate of Botovskaya Cave area provided speleothems more opportunities to grow. This includes also the dry part of the cave, where speleothems younger than in Ledyanaya Lenskaya are found (SB-01112). However, growth breaks separating the calcite/aragonite layers are also present here (Suppl. Fig. 10). Most of the speleothems are composed of aragonite, but some of calcite. Sometimes aragonite and calcite layers are present in the same stalagmite. The thickness of calcite and aragonite horizons usually reaches several cm, and these horizons are separated by hiatuses, as in Ledyanaya Lenskaya Cave (Suppl. Fig. 10).

In Okhotnichya Cave the overall speleothem thickness exceeds 70 cm, showing more intensive speleothem accumulation than in Botovskaya and Ledyanaya Lenskaya Caves. Speleothems are composed of calcite, with smaller amounts of Mg-calcite and aragonite. The petrography of calcite horizons alternating with growth breaks is similar to that found in Ledyanaya Lenskaya and Botovskaya Caves, but the thickness of calcite horizons is larger (Suppl. Fig. 11).

In the Gobi Desert the amounts and thickness of vadose speleothems is smaller. In Shar-Khana Cave a few vadose cave corallites, up to 15 cm thick were found on the walls (Suppl. Fig. 12-I, II). Overgrowths up to 7 cm thick composed of yellow and black calcite layers were found in places on the cave's walls (Suppl. Fig. 12-III). It was difficult to determine if the latter were flowstones or phreatic overgrowth. In Gurvan-Ze'erd the speleothems are mainly phreatic overgrowths 10-30 cm thick. Several stalagmite-like calcite mounds were found on the cave's floor, but their vadose origin (vadose speleothems form above the groundwater table from downward gravity flow of water) is doubtful because their layer morphology more closely resembles the overgrowth pattern of crystallisation from standing water, typical for phreatic calcite (Suppl. Fig 13). All outermost layers of Gurvan-Ze'erd speleothems underwent heating by burning bat guano in the past and therefore were unsuitable for dating, but dating of three deeper and better preserved horizons of these speleothems gave ages >550 ka. In Lovon-Chombo Cave only speleothems of phreatic overgrowth type were found with age >550 ka (Suppl. Fig. 14). Absence of obvious vadose speleothems in the two southernmost caves may indicate permanent aridity since the uplift of these caves above the groundwater level.

Supplementary Figure 9: Speleothems from Ledyanaya Lenskaya Cave: I-II - Stalactite SLL9-2 with 4 growth layers, which youngest layer A is 427 ± 23ka (II - right sample pit). The left sample pit was too deep and crossed into older layer B (dark spot inside the sample pit) yielding a mixed age of 467 ± 10ka. The hiatus between A and B is marked by red fragmented line at the top of layer A and inside the left sample pit (II); III – stalactite SLL9-4 aged ~500 ka. Other speleothems older than U-Th dating limit: are: IV - stalagmite SLL10-6 with 7 growth layers and hiatuses in between; flowstones SLL10-4 (V) and SLL10-8 (VI), and stalactites SLL9-1 (VII), SLL9-3 (VIII) and SLL10-9 (IX).

Supplementary Figure 10: Major speleothems from Botovskaya Cave with their ages in ka: I – stalagmite SB-p6919; II – stalagmite SB-p6929; III - stalagmite SB-p7497; IV – stalagmite SB-p7497-2; V - stalagmite SB-p7497-3; VI – stalagmite SB-p01112.

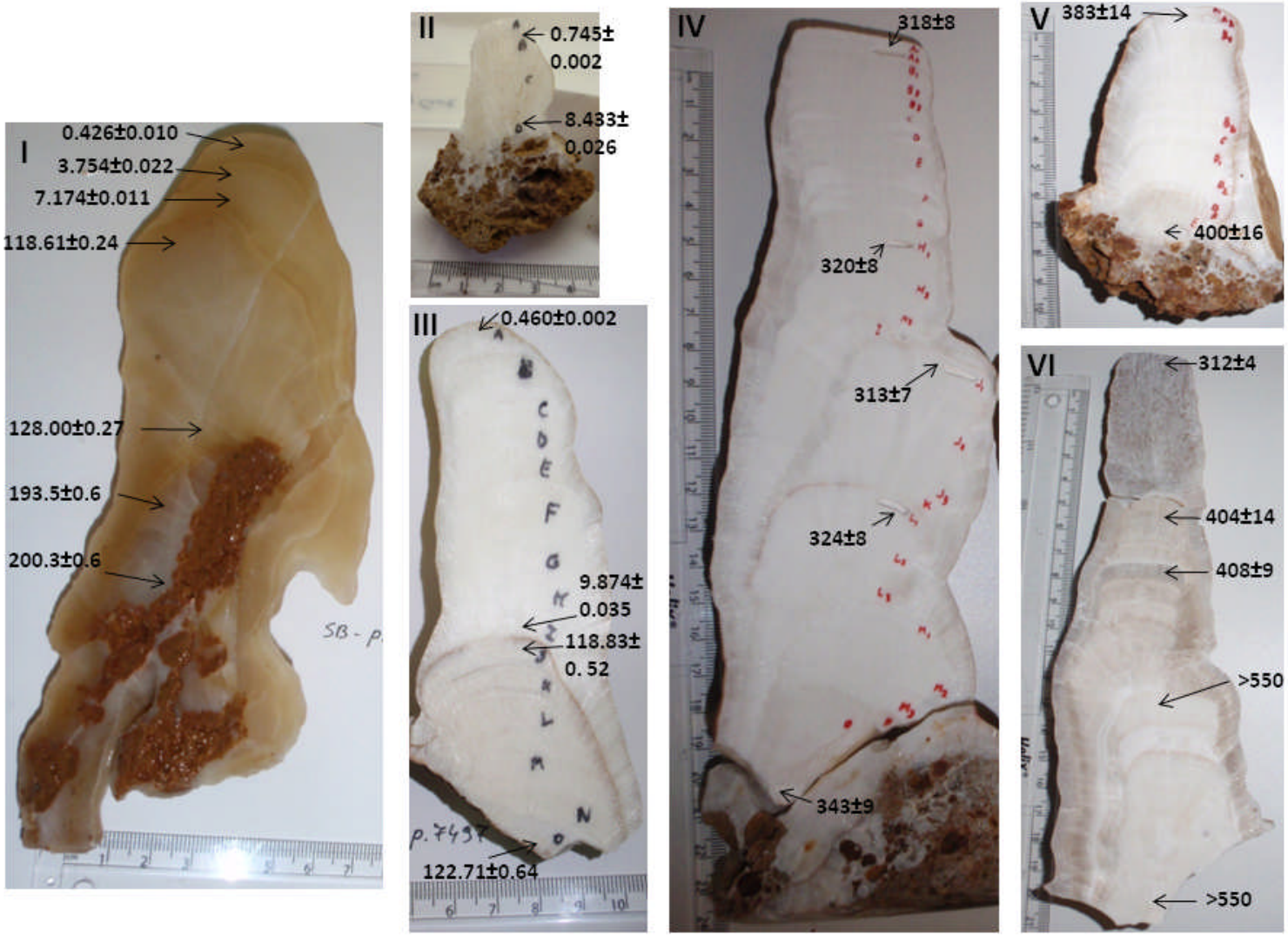

Supplementary Figure 11: Major speleothems from Okhotnichya Cave with their ages in ka: I – stalagmite SOP-2; II – stalagmite SOP-16; III - stalagmite SOP-15; IV – stalagmite SOP-20, cores from tops of stalagmites SOP-18 (V) and SOP-19 (IV).

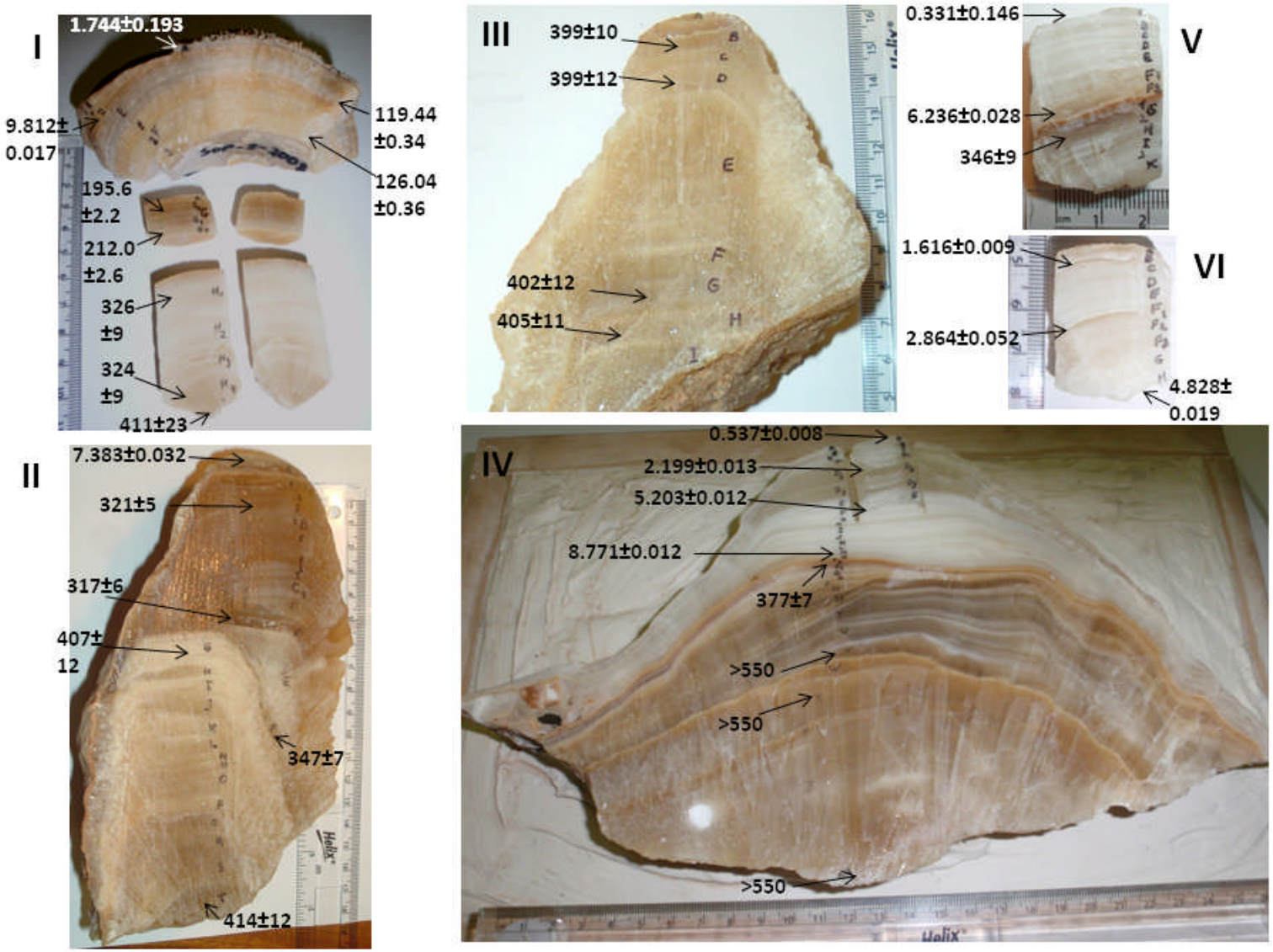

Supplementary Figure 12: Major speleothems from Shar-Khana Cave with their ages in ka: I – corallite MSHK-4; II – corallite MSHK-7; III – phreatic wall overgrowth MSHK-16.

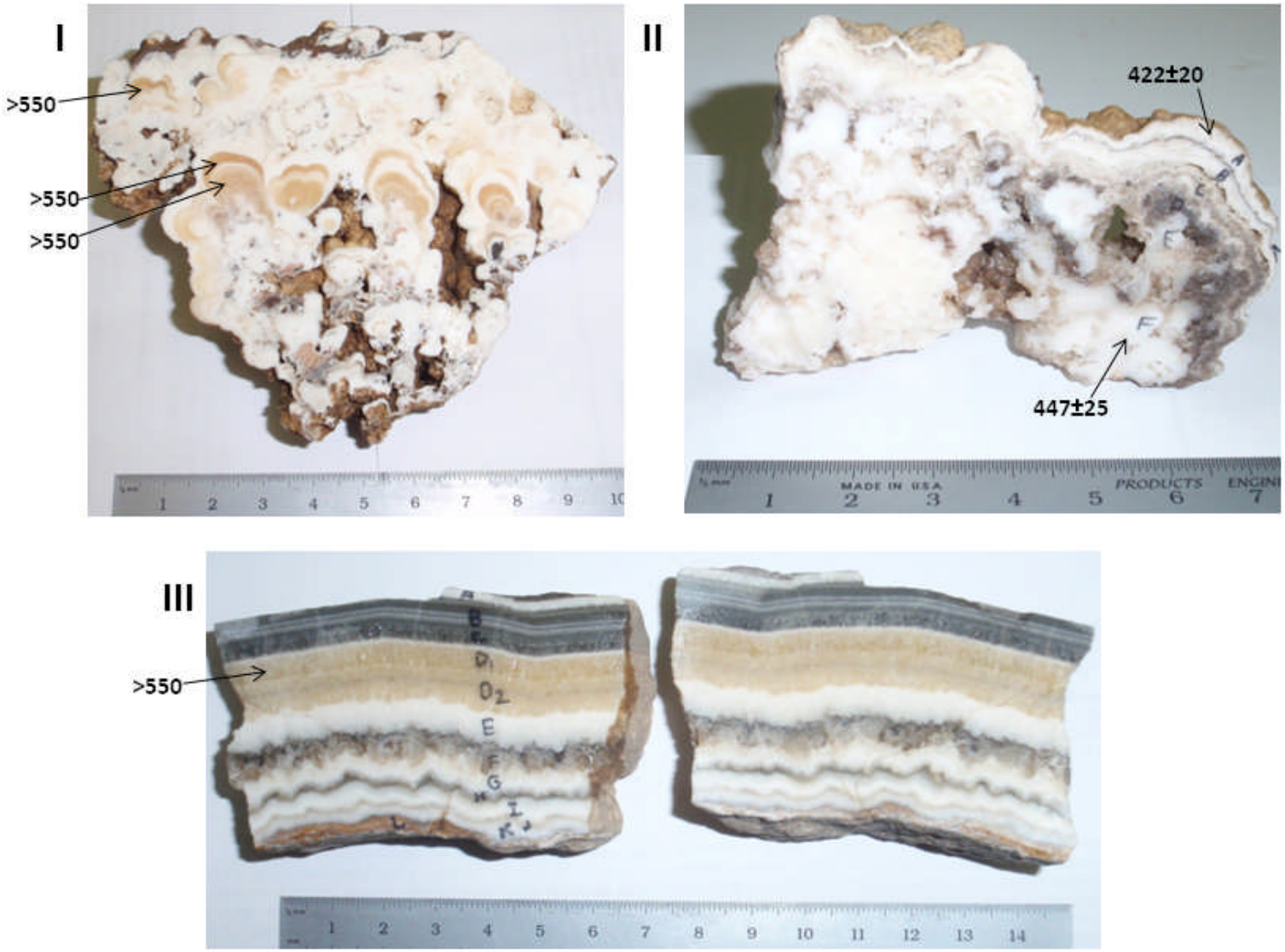

Supplementary Figure 13: Major speleothems from Gurvan Ze'erd Cave: I – stalagmite-like speleothem MGZ-14; II – the broken top of MGZ-14 that was found nearby and showing petrography more resembling a phreatic overgrowth than stalagmite; cores from speleothems MGZ-8 (III) and MGZ-9 (VI) (calcite mounds on the floor). The latter also don't show typical stalagmite stratigraphy and the irregular boundaries between layers may also indicate phreatic conditions. The outer layers of all speleothems in this cave are "baked" by burning bat guano that prevented their dating. Locations of the layers where ages (ka) where determined are shown by arrows.

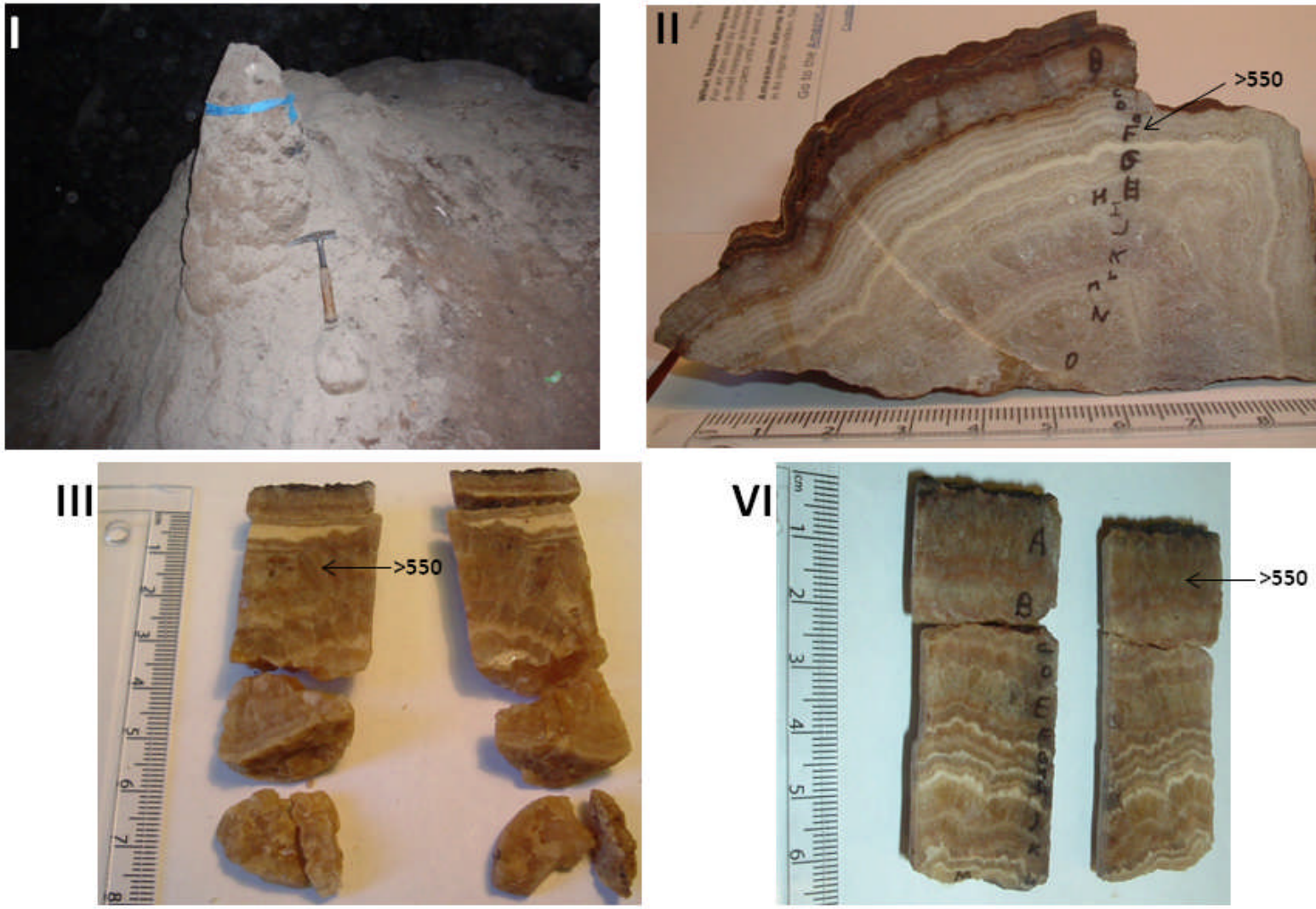

Supplementary Figure 14: Phreatic speleothems from Lovon Chombo Cave (left); a slab of the phreatic overgrowth calcite MLCH-5 which is older than 550 ka (right).

Methods

The speleothems were sectioned using a diamond saw to expose the internal structure and to identify and eliminate diagenetically altered samples by visual inspection. Between 10 and 400 mg of powder was drilled from each sampled horizons using 0.8-1 mm drill bits. Speleothem mineralogy was examined at ETH Zurich, Switzerland, using powder XRD diffractometer (Bruker, AXS D8 Advance), equipped with a scintillation counter and an automatic sampler. Hand specimen inspection shows that all sampled horizons chosen for dating had a typical columnar petrography in calcite and fibrous petrography in aragonite, with almost no voids or re-crystallization marks, suggesting that they are likely have maintained closed system conditions for U-Th isotopes (Suppl. Figs. 9-15).

Supplementary Figure 15: Fibrous petrography of the aragonite layers E and F, and columnar petrography of calcite layer G beneath them in stalagmite SB-01112 (Botovskaya Cave) – A; columnar petrography in layer D of stalagmite SOP-20 (Okhotnichya Cave) – B.

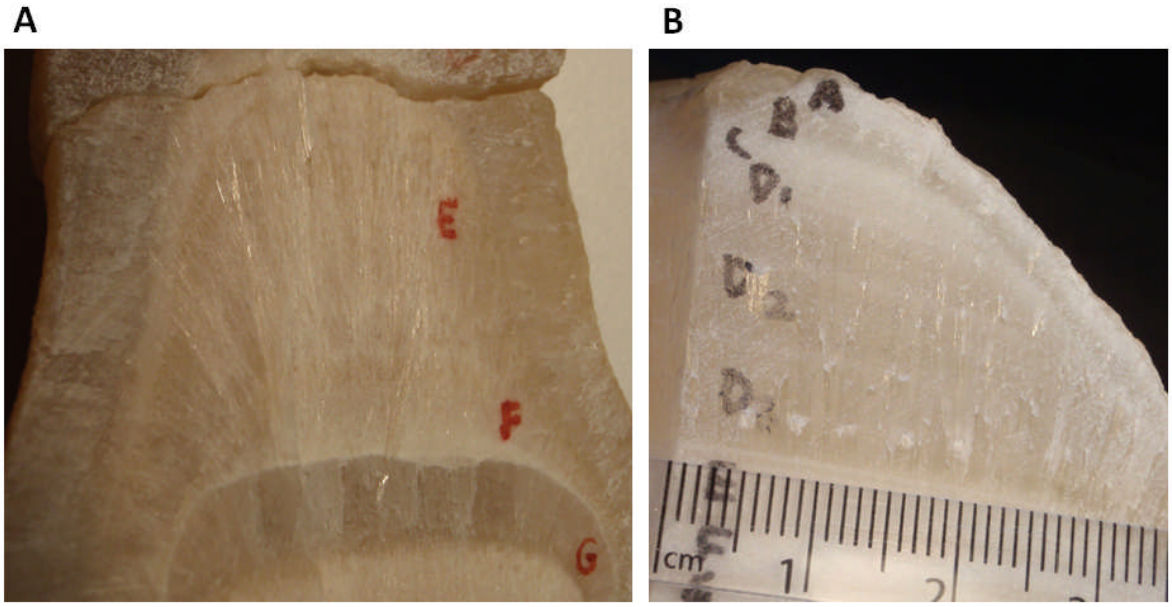

For the U and Th analysis, the samples were spiked with a mixed ^{229}Th-^{236}U spike, dissolved in HNO_3 and refluxed on a hot-plate overnight for spike-sample equilibration. Chemical separation of U and Th from the sample matrix follows procedures adapted from Edwards et al. 1986 (*9*). Measurement of U and Th was performed by Nu-Instrument Multicollector-Inductively-Coupled-Plasma-Mass Spectrometer (MC-ICP-MS) at the University of Oxford. Uranium measurement was performed utilizing Faraday cups for ^{238}U, ^{236}U, and ^{235}U, and ion-counter for the ^{234}U. Abundance sensitivity was corrected based on the half-mass dynamic measurements at 236.5, 235.5, 234.5 and 233.5 on the ion-counter during the initial part of the U measurement. Dynamic Th measurements were performed based on the method of Mason and Henderson (*10*). Major beams ^{238}U, ^{235}U and ^{232}Th were measured on Faraday cups and minor beams of ^{230}Th and ^{229}Th on ion-counter in two steps (^{235}U-^{232}Th-^{230}Th and ^{238}U-^{235}U-^{229}Th); instrumental memory measured in the same configuration before the each sample analysis, and has been corrected for.

Signal noise between the two steps was corrected for by normalising to the respective ^{235}U measurement in each step. Abundance sensitivity was corrected based on the half-mass dynamic measurements at 230.5, 229.5 and 228.5 on the ion-counter during the final part of the Th measurement. Machine biases (ion counter gains and mass fractionation) were corrected using sample-standard bracketing with CRM-145 for U, and two in house ^{229}Th-^{230}Th-^{232}Th standards for Th.

The half-lives of ^{234}U and ^{230}Th used for the age calculation were 245,250 years and 75,690 years respectively according to Cheng et al. (2000) (*11*) and the half-life of ^{238}U was $4.46831*10^{9}$ years according to Jaffey et al. (1971) (*12*). Average system blanks for ^{238}U, ^{232}Th and ^{230}Th were $3.1*10^{-11}$, $1.3*10^{-12}$, $9.1*10^{-16}$ gram respectively. Quoted age uncertainties include the analytical uncertainties, but not the uncertainty in spike calibration.

Dating results and their correction for initial Th were calculated using the Isoplot 4.15 program (*13*) and are presented in Supplementary Table (ST) 1. Speleothem $^{234}U/^{238}U$ and $^{230}Th/^{238}U$ activity ratios are presented in Suppl. Fig. 16. U concentrations in calcite vary between several hundred ppb to tens of ppm, whereas in aragonite they vary from tens to more than 150 ppm. Th concentrations usually vary between 0.5 and 3 ppb, and up to a few tens of ppb in rare cases. Average $^{230}Th/^{232}Th$ activity ratio in the analysed speleothem samples was ~400,000, and only in five Late Holocene speleothem horizons (from total 111 samples) this ratio was below 100. The $^{232}Th/^{238}U$ activity ratios vary between $1.2*10^{-3}$ and $2.7*10^{-7}$ with an average of $7.1*10^{-4}$. Therefore correction for initial Th was small (ST 1), with six ages becoming younger by 150-625 years, whereas all other ages changed by less than 100 years (overall average correction of 27 years). All corrected ages are quoted as before 1950 AD.

To assess the timing of onset and cessation of speleothem growth for important periods, U-Th ages were extrapolated using the OxCal-4.1 program (*14*). Although samples for U-Th analyses were taken as close as possible to growth hiatuses, it is impossible to sample the hiatus itself due to the finite width of samples which must be taken to obtain enough material for U-Th analyses. In addition, sampling at a hiatus risks incorporating a small amount of 'contaminating' material from the other side of the hiatus, therefore samples were taken a small distance from hiatuses.

The age model applied to each speleothem forces all U-Th ages within a speleothem to be in stratigraphic order, with each growth period bounded at the hiatuses with a boundary defining the depth at which growth initiates and finishes. To extrapolate the U-Th ages and hence determine ages for these boundaries the accumulation rate is controlled using a P_Sequence (*15*). The P_Sequence is a semi-quantitive control on the variability of the accumulation rate achived by inserting aditional age control points within the sequence which must also obey stratigraphic order. The greater the number of additional control points per unit length (k) the more linear the age model is forced to be. A k value of 1.5 (depth units were in cm) was chosen because this gave a good agreement with the U-Th data, where multiple U-Th data were available between hiatuses. A greater k value would result in more linear accumulation rates, and higher precision

estimates of the boundary ages, but would produce age models which were not in agreement with the variability of sedimentation rates observed in the U-Th data.

Supplementary Figure 16: $^{234}U/^{238}U$ and $^{230}Th/^{238}U$ activity ratios of Siberian and Mongolian speleothems with their 2σ error bars ^{230}Th (shown in red), based on raw data from Supplementary Table 1 (not corrected for initial ^{230}Th). The black lines show the paths of radioactive decay for various initial $^{234}U/^{238}U$ activity ratios when the initial $^{230}Th/^{238}U$ activity ratio is 0. Note the very high ($^{234}U/^{238}U$) ratios of many samples, and the lack of samples in the "forbidden zone" in the bottom right of the figure.

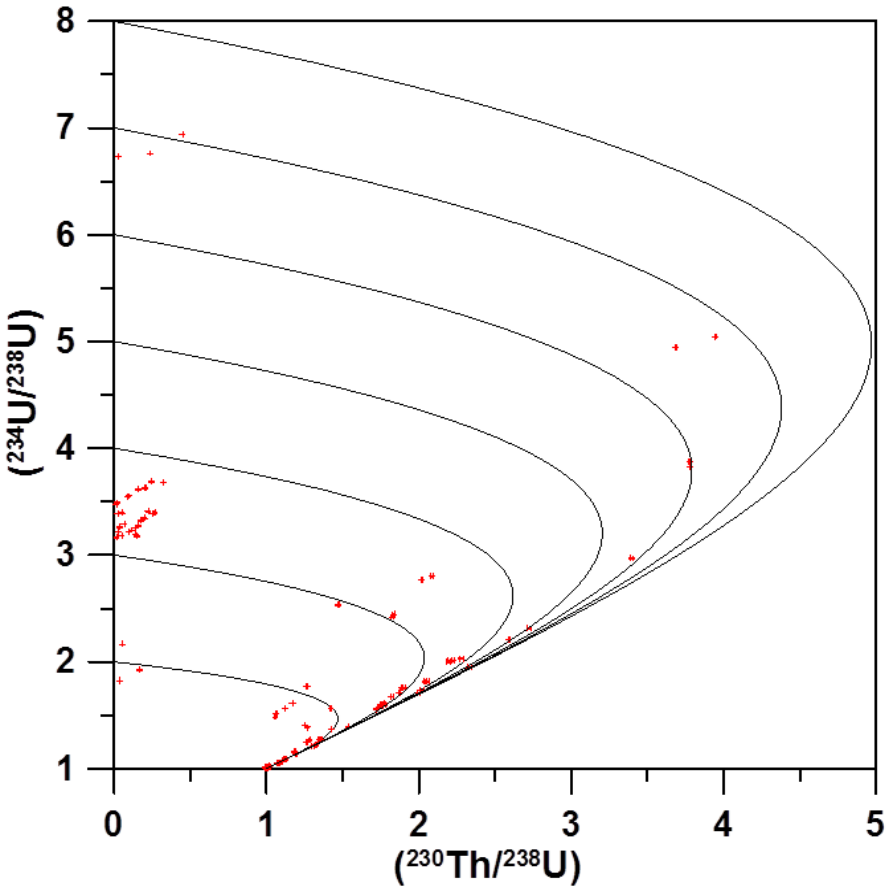

To further constrain the ages of boundaries determined by the age modelling approach, the boundaries in separate speleothems corresponding to the same growth period are assumed to be the same age. This additional constraint is only applied when the ages of the boundaries were within 2σ error of each other. This is a reasonable constraint considering the proposed regional control on speleothem growth. Where speleothem growth was clearly dependent on a local rather than a regional control, the affected boundary for that speleothem was not used to determine the timings of growth for that interglacial. For example: for stalagmites SB-7497 and SB-6929 only the top boundary age is consistent with a regional climatic control, whereas the bottom boundary was affected by local control (they started growing on the collapsed sediments much later then the beginning of the MIS-5.5 (SB-7497) or Holocene (SB-6929)).

The results of the OxCal-4.1calculations were applied for Holocene and MIS-5.5 interglacial boundary ages. They are shown in ST-2 and ST-3 and also given as grey rectangles in Fig. 3. For older interglacials the growth periods are shown as the range of U-Th ages.

Additional References of GICC05 record - (*16-19*).

Supplementary References and Notes:

1. Philip's, Ed., *Modern School Atlas, 95-th edition*, (Philip's, a division of Octopus Publishing Group Limited, London, 2007).
2. E. D. Ershov, in *Geocriological map of the USSR, 1:2500000 (in Russian)*. (Ministry of Geology of USSR and Moscow State University, Moscow, 1991).
3. D. Ford, P. W. Williams, *Karst Geomorphology and Hydrology*. (Unwin Hyman, London, 1989), pp. 601 pp.
4. A. G. Filippov, in *Enisey Province, Almanac*. (Krasnoyarsk Territorial Museum of Local History, Krasnoyarsk, Russia, 2009), vol. Issue 4, pp. 168-175.
5. A. A. Bukharow *et al.*, *Atlas: Lake Baikal, past, present, future*. N. S. Owchinnikova, Ed., (FGUP Eastern Siberian Aero-Geodesic Corporation, Irkutsk 664000, Russia, 2005).
6. D. Lacelle, B. Lauriol, I. D. Clark, *Journal of Cave and Karst Studies* **71**, 48 (2009).
7. D. Dorjotov, N. Orshikh, T. Oyunchimeg, *Geographic Atlas of Mongolian Republic (in Mongolian)*. (Mongolian Institute of Geodesy and Cartography Ulaanbaatar, Mongolia, 2004), pp. 64.
8. E. Avirmed, *The Caves of Mongolia (In Mongolian, Russian/English abstracts)*. S. Tzegmid, P. Tzolmon, Eds., (Academy of Sciences of Mongolian Republic, Ulaan-Baatar, 1999), pp. 206.
9. L. R. Edwards, J. H. Chen, G. J. Wasserburg, *Earth and Planetary Science Letters* **81**, 175 (1987).
10. A. J. Mason, G. M. Henderson, *International Journal of Mass Spectrometry* **295**, 26 (2010).
11. H. Cheng, L. R. Edwards, C. Hoff, C. D. Gallup, Y. Richards, *Chemical Geology* **169**, 17 (2000).
12. A. H. Jaffey, K. F. Flynn, L. E. Glendenin, W. C. Bentley, A. M. Essling, *Physical Review C* **4**, 1889 (1971).
13. K. A. Ludwig, Ed., *User's Manual for Isoplot 3.75-4.15, a Geochronological Toolkit for Microsoft Excel*, vol. 5 (Berkeley Geochronological Centre, Berkeley CA, USA, 2012), vol. 5.
14. C. B. Ramsey, *Radiocarbon* **51**, 337 (2009).
15. C. B. Ramsey, *Quaternary Science Reviews* **27**, 42 (2008).
16. K. K. Andersen *et al.*, *Quaternary Science Reviews* **25**, 3246 (2006).
17. S. O. Rasmussen *et al.*, *Quaternary Science Reviews* **27**, 18 (2008).
18. A. Svensson *et al.*, *Quaternary Science Reviews* **25**, 3258 (2006).
19. B. M. Vinther *et al.*, *J. Geophys. Res.* **111**, D13102 (2006).
20. C. B. Ramsey, *Radiocarbon* **37**, 425 (1995).

Supplementary Table 1, page 1.

Nu.	Cave	Sample	^{238}U (ppm)	^{232}Th (ppb)	$(^{230}Th/^{232}Th)$	$(^{232}Th/^{238}U)$	2σ abs	$(^{230}Th/^{238}U)$	2σ abs	$(^{234}U/^{238}U)$	2σ abs	Raw Age (ka before 2010 A.D.)	2σ	$(^{230}Th/^{238}U)$ corr.	2σ abs	$(^{234}U/^{238}U)$ corr.	2σ abs	$(^{234}U/^{238}U)$ initial*	Age corr. (ka before 2010 A.D.)	2σ	**Age (ka before 1950 A.D.)**	**2σ**
1	Lenskaya Ledyanaya	SLL9-1-B	23.65	1.78	41232	2.46E-05	3.21E-08	1.02131	0.00133	1.01355	0.00115	>550	n/a	1.02131	0.00133	1.01355	0.00115		>550	n/a	**>550**	**n/a**
2	Lenskaya Ledyanaya	SLL9-1-C	22.60	1.79	39159	2.59E-05	3.44E-08	1.01983	0.00135	1.01292	0.00115	>550	n/a	1.01983	0.00135	1.01292	0.00115		>550	n/a	**>550**	**n/a**
3	Lenskaya Ledyanaya	SLL9-2-A	28.77	44.91	2621	5.11E-04	1.48E-05	1.34467	0.00479	1.26992	0.00416	427	23	1.34482	0.00479	1.27004	0.00416	1.90279	427	23	**427**	**23**
4	Lenskaya Ledyanaya	SLL9-2-A+B **	28.76	7.50	15848	8.54E-05	1.12E-07	1.36002	0.00177	1.27251	0.00115	467	10	1.36004	0.00177	1.27253	0.00115	2.01951	467	10	**467**	**10**
5	Lenskaya Ledyanaya	SLL9-2-D	29.58	1.67	60547	1.85E-05	2.47E-08	1.12533	0.00150	1.09017	0.00115	>550	n/a	1.12533	0.00150	1.09017	0.00115		>550	n/a	**>550**	**n/a**
6	Lenskaya Ledyanaya	SLL9-3-A	9.49	0.96	32546	3.30E-05	4.48E-08	1.08892	0.00148	1.04965	0.00115	>550	n/a	1.08892	0.00148	1.04965	0.00115		>550	n/a	**>550**	**n/a**
7	Lenskaya Ledyanaya	SLL9-3-D	34.70	0.56	188674	5.29E-06	6.93E-09	1.01659	0.00133	1.01659	0.00115	>550	n/a	1.01659	0.00133	1.01659	0.00115		545	36	**545**	**36**
8	Lenskaya Ledyanaya	SLL9-3-E	34.66	1.34	66205	1.27E-05	7.02E-08	1.01879	0.00386	1.01672	0.00098	>550	n/a	1.01879	0.00386	1.01672	0.00098		>550	n/a	**>550**	**n/a**
9	Lenskaya Ledyanaya	SLL9-3-G	14.83	0.42	106891	9.28E-06	1.21E-08	1.01692	0.00132	1.01353	0.00115	>550	n/a	1.01692	0.00132	1.01353	0.00115		>550	n/a	**>550**	**n/a**
10	Lenskaya Ledyanaya	SLL9-4-B	27.53	0.87	96816	1.04E-05	1.33E-08	1.01772	0.00130	1.01852	0.00115	524	28	1.01772	0.00130	1.01852	0.00115		524	28	**524**	**28**
11	Lenskaya Ledyanaya	SLL9-4-C	23.58	2.63	27718	3.65E-05	4.68E-08	1.01631	0.00130	1.01915	0.00115	499	22	1.01631	0.00130	1.01915	0.00115		499	22	**499**	**22**
12	Lenskaya Ledyanaya	SLL10-4-A	27.70	20.67	4842	2.44E-04	8.44E-07	1.19427	0.00412	1.13799	0.00156	>550	n/a	1.19431	0.00412	1.13802	0.00157		>550	n/a	**>550**	**n/a**
13	Lenskaya Ledyanaya	SLL10-6-A	43.22	13.07	13289	9.90E-05	2.74E-07	1.32480	0.00366	1.21627	0.00156	>550	n/a	1.32482	0.00366	1.21628	0.00156		>550	n/a	**>550**	**n/a**
14	Lenskaya Ledyanaya	SLL10-8-A	44.55	12.76	11671	9.37E-05	2.27E-07	1.11027	0.00268	1.07921	0.00156	>550	n/a	1.11028	0.00268	1.07921	0.00156		>550	n/a	**>550**	**n/a**
15	Lenskaya Ledyanaya	SLL10-9-A	21.31	4.09	18781	6.28E-05	6.34E-06	1.12320	0.00630	1.08883	0.00336	>550	n/a	1.12321	0.00630	1.08883	0.00336		>550	n/a	**>550**	**n/a**
16	Lenskaya Ledyanaya	SLL10-9-Bbot	26.60	0.77	97372	9.45E-06	9.53E-07	1.07615	0.00588	1.05056	0.00336	>550	n/a	1.07615	0.00588	1.05056	0.00336		>550	n/a	**>550**	**n/a**
17	Botovskaya	SB-p01112-A	0.46	1.81	2623	1.28E-03	1.24E-05	3.39786	0.01123	2.96769	0.00278	312	4	3.40040	0.01131	2.96978	0.00299	5.76270	312	4	**312**	**4**
18	Botovskaya	SB-p1112-E	38.13	0.26	281855	2.25E-06	2.27E-07	2.72593	0.01496	2.31146	0.00336	404	14	2.72593	0.01496	2.31146	0.00336	5.10509	404	14	**404**	**14**
19	Botovskaya	SB-p01112-G	1.01	0.04	123369	1.41E-05	1.35E-07	2.59411	0.00790	2.20924	0.00278	408	9	2.59412	0.00790	2.20926	0.00278	4.83184	408	9	**408**	**9**
20	Botovskaya	SB-p1112-N	77.70	3.68	165292	1.55E-05	1.56E-06	2.33323	0.01325	1.94838	0.00336	>550	n/a	2.33325	0.01325	1.94840	0.00336		>550	n/a	**>550**	**n/a**
21	Botovskaya	SB-p1112-Ptop	52.65	0.89	1092598	5.51E-06	5.55E-07	1.99947	0.01121	1.70759	0.00336	>550	n/a	1.99948	0.01121	1.70760	0.00336		>550	n/a	**>550**	**n/a**
22	Botovskaya	SB-p1112-Pbot	68.57	5.43	74670	2.59E-05	2.61E-06	2.02192	0.01111	1.73231	0.00336	>550	n/a	2.02194	0.01111	1.73233	0.00336		>550	n/a	**>550**	**n/a**
23	Botovskaya	SB-p6915-B	3.51	1.02	10241	9.54E-05	9.15E-07	1.00023	0.00304	1.00772	0.00278	496	60	1.00023	0.00304	1.00772	0.00278		496	61	**496**	**61**
24	Botovskaya	SB-p6919-A1	0.73	3.08	24	1.39E-03	9.71E-06	0.03120	0.00004	6.73293	0.00156	0.505	0.001	0.03009	0.00063	6.73950	0.00365	6.7474	0.486	0.010	**0.426**	**0.010**
25	Botovskaya	SB-p6919-Btop	0.62	6.34	71	3.36E-03	6.16E-06	0.23669	0.00035	6.75991	0.00094	3.858	0.006	0.23457	0.00132	6.77594	0.00812	6.8385	3.814	0.022	**3.754**	**0.022**
26	Botovskaya	SB-p6919-Bbot	0.73	1.96	511	8.77E-04	1.53E-06	0.45105	0.00062	6.93818	0.00094	7.24	0.01	0.45065	0.00068	6.94249	0.00236	7.0652	7.234	0.011	**7.174**	**0.011**
27	Botovskaya	SB-p6919-C1	0.68	1.77	4300	8.51E-04	1.08E-06	3.68608	0.00464	4.94461	0.00094	118.68	0.23	3.68797	0.00474	4.94739	0.00169	6.5204	118.67	0.24	**118.61**	**0.24**
28	Botovskaya	SB-p6919-C4	1.02	2.17	5560	6.99E-04	8.79E-07	3.94775	0.00494	5.04202	0.00094	128.07	0.26	3.94946	0.00501	5.04435	0.00151	6.8082	128.06	0.27	**128.00**	**0.27**
29	Botovskaya	SB-p6919-D1	0.70	2.55	3134	1.20E-03	1.48E-06	3.77892	0.00465	3.87977	0.00094	193.6	0.5	3.78168	0.00486	3.88263	0.00173	5.9815	193.5	0.6	**193.5**	**0.6**
30	Botovskaya	SB-p6919-D2	0.89	3.99	2568	1.47E-03	1.82E-06	3.78561	0.00466	3.82684	0.00094	200.4	0.5	3.78900	0.00497	3.83027	0.00199	5.9861	200.4	0.6	**200.3**	**0.6**
31	Botovskaya	SB-p6929-top	54.53	5.76	722	3.46E-05	2.58E-07	0.02505	0.00007	3.38920	0.00070	0.806	0.002	0.02502	0.00007	3.38926	0.00070	3.3947	0.805	0.002	**0.745**	**0.002**
32	Botovskaya	SB-p6929-bot	102.45	12.03	6560	3.85E-05	1.14E-07	0.25639	0.00076	3.38385	0.00070	8.494	0.026	0.25637	0.00076	3.38393	0.00070	3.4418	8.493	0.026	**8.433**	**0.026**
33	Botovskaya	SB-p7497-A1	94.09	6.14	746	2.14E-05	1.61E-07	0.01662	0.00005	3.47526	0.00070	0.521	0.002	0.01660	0.00005	3.47530	0.00070	3.4789	0.520	0.002	**0.460**	**0.002**
34	Botovskaya	SB-p7497-I	158.12	0.13	385301	2.68E-07	9.00E-10	0.32416	0.00109	3.67570	0.00070	9.93	0.03	0.32416	0.00109	3.67570	0.00070	3.7519	9.934	0.035	**9.874**	**0.035**
35	Botovskaya	SB-p7497-J	88.34	1.38	509387	5.10E-06	1.40E-08	2.01878	0.00554	2.76532	0.00070	118.89	0.52	2.01878	0.00554	2.76532	0.00070	3.4703	118.89	0.52	**118.83**	**0.52**
36	Botovskaya	SB-p7497-O	35.96	1.51	134890	1.37E-05	4.40E-08	2.08760	0.00668	2.80083	0.00070	122.77	0.637	2.08761	0.00668	2.80085	0.00070	3.5478	122.77	0.64	**122.71**	**0.64**
37	Botovskaya	SB-p7497-2-A2	140.54	0.28	6078550	6.52E-07	6.57E-08	2.19811	0.01260	1.99783	0.00336	318	8	2.19811	0.01260	1.99783	0.00336	3.4523	318	8	**318**	**8**
38	Botovskaya	SB-p7497-2-H1	126.46	0.60	14276136	1.55E-06	1.57E-07	2.19701	0.01253	1.99474	0.00336	320	8	2.19701	0.01253	1.99474	0.00336	3.4561	320	8	**320**	**8**
39	Botovskaya	SB-p7497-2-J1	146.88	0.99	3795917	2.22E-06	2.23E-07	2.20363	0.01217	2.00929	0.00336	313	7	2.20363	0.01217	2.00929	0.00336	3.4452	313	7	**313**	**7**
40	Botovskaya	SB-p7497-2-L1	132.19	0.77	12343271	1.91E-06	1.93E-07	2.22469	0.01244	2.01122	0.00336	324	8	2.22470	0.01244	2.01122	0.00336	3.5263	324	8	**324**	**8**
41	Botovskaya	SB-p7497-2-Obot	99.16	0.21	730849	6.77E-07	6.83E-08	2.27791	0.01263	2.02957	0.00336	343	9	2.27791	0.01263	2.02957	0.00336	3.7159	343	9	**343**	**9**
42	Botovskaya	SB-p7497-3-A2	101.49	0.31	133444	9.95E-07	1.00E-07	2.04212	0.01123	1.81259	0.00336	383	14	2.04212	0.01123	1.81259	0.00336	3.3976	383	14	**383**	**14**
43	Botovskaya	SB-p7497-3-Ebot	89.54	0.73	158503	2.69E-06	2.71E-07	2.05694	0.01136	1.81236	0.00336	400	16	2.05695	0.01136	1.81236	0.00336	3.5175	400	16	**400**	**16**

Supplementary Table 1, page 2.

Nu.	Cave	Sample	^{238}U (ppm)	^{232}Th (ppb)	$(^{230}Th/^{232}Th)$	$(^{232}Th/^{238}U)$	2σ abs	$(^{230}Th/^{238}U)$	2σ abs	$(^{234}U/^{238}U)$	2σ abs	Raw Age (ka before 2010 A.D.)	2σ	$(^{230}Th/^{238}U)$ corr.	2σ abs	$(^{234}U/^{238}U)$ corr.	2σ abs	$(^{234}U/^{238}U)$ initial*	Age corr. (ka before 2010 A.D.)	2σ	**Age (ka before 1950 A.D.)**	**2σ**
44	Okhotnichya	SOP-1-B	3.95	5.81	2994	4.81E-04	4.97E-06	1.42283	0.00484	1.56038	0.00114	199.6	1.7	1.42300	0.00485	1.56060	0.00115	1.98534	199.5	1.7	**199.5**	**1.7**
45	Okhotnichya	SOP-1-D (II)	4.76	0.14	134213	9.30E-06	1.53E-08	1.42508	0.00212	1.36532	0.00098	342	3	1.42508	0.00212	1.36532	0.00098	1.96060	342	3	**342**	**3**
46	Okhotnichya	SOP-2-A	4.10	81.38	5	6.49E-03	1.57E-05	0.03527	0.00121	1.82091	0.00166	2.124	0.073	0.03006	0.00318	1.82534	0.00309	1.82956	1.804	0.193	**1.744**	**0.193**
47	Okhotnichya	SOP-2-D	4.88	0.88	2776	5.89E-05	9.05E-08	0.16798	0.00027	1.92249	0.00098	9.874	0.017	0.16794	0.00027	1.92253	0.00098	1.94863	9.872	0.017	**9.812**	**0.017**
48	Okhotnichya	SOP-2-Etop	4.19	0.74	17883	5.77E-05	8.47E-08	1.06420	0.00160	1.51644	0.00098	119.5	0.3	1.06420	0.00160	1.51647	0.00098	1.72397	119.50	0.34	**119.44**	**0.34**
49	Okhotnichya	SOP-2-Ebot	4.37	1.99	7026	1.49E-04	2.18E-07	1.05714	0.00160	1.48357	0.00098	123.1	0.4	1.05715	0.00160	1.48363	0.00098	1.68486	123.09	0.36	**123.03**	**0.36**
50	Okhotnichya	SOP-2-F1	4.27	3.94	3690	3.02E-04	4.45E-07	1.12274	0.00170	1.55927	0.00098	124.3	0.4	1.12277	0.00171	1.55941	0.00099	1.79477	124.25	0.36	**124.19**	**0.36**
51	Okhotnichya	SOP-2-F3	4.86	1.49	11433	1.01E-04	1.48E-07	1.17356	0.00177	1.61095	0.00098	126.1	0.4	1.17357	0.00178	1.61101	0.00098	1.87262	126.10	0.36	**126.04**	**0.36**
52	Okhotnichya	SOP-2-G2	6.23	0.17	120620	8.70E-06	2.52E-07	1.25301	0.00366	1.40668	0.00416	195.6	2.2	1.25301	0.00366	1.40669	0.00416	1.70694	195.6	2.2	**195.6**	**2.2**
53	Okhotnichya	SOP-2-G3	3.79	1.65	8789	1.43E-04	4.13E-06	1.27002	0.00370	1.38516	0.00416	212.1	2.6	1.27005	0.00370	1.38520	0.00416	1.70145	212.1	2.6	**212.0**	**2.6**
54	Okhotnichya	SOP-2-H1top	3.54	0.33	37547	3.08E-05	8.92E-07	1.28435	0.00373	1.26462	0.00416	326	9	1.28436	0.00373	1.26462	0.00416	1.66453	326	9	**326**	**9**
55	Okhotnichya	SOP-2-H4bot	4.67	0.44	36269	3.08E-05	8.93E-07	1.26236	0.00367	1.24815	0.00416	324	9	1.26237	0.00367	1.24816	0.00416	1.62041	324	9	**324**	**9**
56	Okhotnichya	SOP-2-I	4.51	2.93	5545	2.13E-04	6.16E-06	1.18610	0.00344	1.15594	0.00416	411	22	1.18613	0.00344	1.15596	0.00416	1.49846	411	22	**411**	**22**
57	Okhotnichya	SOP-3-B	0.27	1.68	655	2.02E-03	7.90E-06	1.30426	0.00579	1.21316	0.00024	>550	n/a	1.30477	0.00582	1.21351	0.00051		>550	n/a	**>550**	**n/a**
58	Okhotnichya	SOP-6-A1	0.40	9.03	140	7.35E-03	3.04E-05	1.01166	0.00347	1.01306	0.00003	546	73	1.01173	0.00381	1.01314	0.00153		545	92	**545**	**92**
59	Okhotnichya	SOP-11-A	0.82	2.39	1059	9.51E-04	5.23E-06	0.99527	0.00368	1.01421	0.00003	407	17	0.99527	0.00369	1.01422	0.00020	1.04489	407	18	**407**	**18**
60	Okhotnichya	SOP-15-B-low	1.27	1.43	4765	3.68E-04	3.53E-06	1.76224	0.00534	1.59181	0.00278	399	10	1.76248	0.00534	1.59199	0.00279	2.82747	399	10	**399**	**10**
61	Okhotnichya	SOP-15-D	1.59	2.31	3708	4.77E-04	1.38E-05	1.77990	0.00515	1.60476	0.00416	399	12	1.78021	0.00516	1.60500	0.00417	2.87092	399	12	**399**	**12**
62	Okhotnichya	SOP-15-G	1.56	0.88	9544	1.86E-04	5.37E-06	1.77888	0.00514	1.60248	0.00416	402	12	1.77900	0.00514	1.60258	0.00416	2.87952	402	12	**402**	**12**
63	Okhotnichya	SOP-15-H	1.73	0.97	9543	1.84E-04	1.77E-06	1.77264	0.00537	1.59660	0.00278	405	11	1.77276	0.00537	1.59669	0.00278	2.87437	405	11	**405**	**11**
64	Okhotnichya	SOP-16-A	1.70	4.22	308	8.13E-04	2.99E-06	0.24616	0.00090	3.68366	0.00544	7.462	0.030	0.24566	0.00095	3.68547	0.00552	3.74255	7.443	0.032	**7.383**	**0.032**
65	Okhotnichya	SOP-16-B3	1.81	0.27	35559	4.83E-05	4.64E-07	1.90303	0.00578	1.75890	0.00278	321	5	1.90307	0.00578	1.75893	0.00278	2.88277	321	5	**321**	**5**
66	Okhotnichya	SOP-16-D	2.74	40.21	393	4.81E-03	1.39E-04	1.89155	0.00547	1.75410	0.00416	318	5	1.89510	0.00586	1.75711	0.00455	2.85689	317	6	**317**	**6**
67	Okhotnichya	SOP-16-F	3.41	0.29	66187	2.80E-05	8.12E-07	1.87074	0.00541	1.70916	0.00416	347	7	1.87076	0.00541	1.70917	0.00416	2.88877	347	7	**347**	**7**
68	Okhotnichya	SOP-16-G2-top	1.20	0.72	8735	1.97E-04	5.70E-06	1.73262	0.00500	1.56562	0.00416	407	13	1.73273	0.00501	1.56571	0.00416	2.78810	407	13	**407**	**13**
69	Okhotnichya	SOP-16-T	2.80	0.56	25827	6.53E-05	6.26E-07	1.72275	0.00524	1.55527	0.00278	414	12	1.72279	0.00524	1.55530	0.00278	2.78914	414	12	**414**	**12**
70	Okhotnichya	SOP-17-E1	0.19	0.32	1835	5.51E-04	3.88E-06	1.00548	0.00514	1.00842	0.00001	>550	n/a	1.00548	0.00515	1.00842	0.00011		>550	n/a	**>550**	**n/a**
71	Okhotnichya	SOP-18-A	0.85	25.84	2	9.92E-03	2.32E-05	0.02071	0.00109	3.48837	0.00504	0.647	0.034	0.01261	0.00471	3.50895	0.01173	3.51172	0.391	0.146	**0.331**	**0.146**
72	Okhotnichya	SOP-18-F2	1.48	3.68	256	8.13E-04	3.38E-06	0.20595	0.00079	3.62683	0.00532	6.316	0.027	0.20542	0.00085	3.62860	0.00540	3.67579	6.296	0.028	**6.236**	**0.028**
73	Okhotnichya	SOP-18-G	2.09	0.49	23707	7.62E-05	5.77E-06	1.82321	0.00959	1.67296	0.00136	346	9	1.82326	0.00959	1.67300	0.00136	2.78779	346	9	**346**	**9**
74	Okhotnichya	SOP-19-B	1.22	0.50	391	1.33E-04	1.27E-06	0.05215	0.00025	3.39690	0.00486	1.680	0.008	0.05205	0.00025	3.39716	0.00486	3.40854	1.676	0.009	**1.616**	**0.009**
75	Okhotnichya	SOP-19-F1	1.23	0.41	861	1.09E-04	1.11E-05	0.09454	0.00165	3.54963	0.00278	2.93	0.05	0.09445	0.00165	3.54986	0.00278	3.57102	2.924	0.052	**2.864**	**0.052**
76	Okhotnichya	SOP-19-H	1.65	1.90	430	3.76E-04	1.89E-06	0.16011	0.00054	3.61781	0.00530	4.90	0.02	0.15985	0.00056	3.61862	0.00532	3.65505	4.888	0.019	**4.828**	**0.019**
77	Okhotnichya	SOP-20-A	0.64	0.72	51	3.69E-04	1.44E-06	0.01764	0.00017	3.16366	0.00241	0.608	0.006	0.01734	0.00024	3.16432	0.00244	3.16798	0.597	0.008	**0.537**	**0.008**
78	Okhotnichya	SOP-20-B	0.67	0.24	265	1.17E-04	5.99E-07	0.03081	0.00039	3.21976	0.00122	1.044	0.013	0.03071	0.00039	3.21998	0.00122	3.22652	1.041	0.013	**0.981**	**0.013**
79	Okhotnichya	SOP-20-C	0.83	0.25	410	9.81E-05	5.03E-07	0.04018	0.00051	3.26408	0.00597	1.345	0.017	0.04011	0.00051	3.26427	0.00597	3.27288	1.343	0.017	**1.283**	**0.017**
80	Okhotnichya	SOP-20-D1	0.89	0.40	351	1.46E-04	1.01E-06	0.05147	0.00102	3.17922	0.00122	1.772	0.035	0.05135	0.00102	3.17948	0.00122	3.19040	1.768	0.035	**1.708**	**0.035**
81	Okhotnichya	SOP-20-D2.1	0.95	0.32	626	1.08E-04	2.96E-07	0.06788	0.00037	3.29054	0.00122	2.262	0.013	0.06780	0.00038	3.29075	0.00122	3.30542	2.259	0.013	**2.199**	**0.013**
82	Okhotnichya	SOP-20-D2.2	0.96	0.88	322	3.01E-04	8.25E-07	0.09653	0.00053	3.21470	0.00122	3.305	0.018	0.09630	0.00055	3.21526	0.00125	3.23599	3.296	0.019	**3.236**	**0.019**
83	Okhotnichya	SOP-20-D3.1	1.01	0.64	549	2.07E-04	4.43E-07	0.11398	0.00025	3.23234	0.00122	3.889	0.009	0.11383	0.00026	3.23273	0.00123	3.25737	3.883	0.009	**3.823**	**0.009**
84	Okhotnichya	SOP-20-D3.2	1.22	0.26	1938	7.01E-05	1.46E-07	0.13793	0.00029	3.25024	0.00122	4.694	0.010	0.13788	0.00030	3.25037	0.00122	3.28041	4.692	0.010	**4.632**	**0.010**
85	Okhotnichya	SOP-20-E1	1.34	0.15	3903	3.55E-05	7.50E-08	0.14296	0.00031	3.19777	0.00122	4.950	0.011	0.14294	0.00031	3.19784	0.00122	3.22879	4.949	0.011	**4.889**	**0.011**
86	Okhotnichya	SOP-20-E	1.36	0.61	1025	1.47E-04	7.17E-07	0.14971	0.00052	3.17493	0.00441	5.226	0.020	0.14961	0.00053	3.17519	0.00441	3.20753	5.222	0.020	**5.162**	**0.020**
87	Okhotnichya	SOP-20-E2	1.25	0.30	1948	7.92E-05	1.66E-07	0.15547	0.00033	3.27263	0.00122	5.265	0.012	0.15541	0.00033	3.27278	0.00122	3.30684	5.263	0.012	**5.203**	**0.012**
88	Okhotnichya	SOP-20-H	1.14	0.51	1195	1.47E-04	4.24E-06	0.17811	0.00053	3.32116	0.00416	5.958	0.020	0.17801	0.00054	3.32144	0.00416	3.36084	5.954	0.020	**5.894**	**0.020**
89	Okhotnichya	SOP-20-J1	1.25	0.73	1034	1.92E-04	5.57E-06	0.20147	0.00060	3.34753	0.00416	6.705	0.022	0.20135	0.00060	3.34791	0.00417	3.39279	6.700	0.022	**6.640**	**0.022**
90	Okhotnichya	SOP-20-K	1.26	0.68	1251	1.78E-04	5.17E-06	0.22512	0.00067	3.40800	0.00416	7.376	0.024	0.22501	0.00067	3.40835	0.00417	3.45905	7.371	0.024	**7.311**	**0.024**
91	Okhotnichya	SOP-20-M	1.34	0.71	1500	1.74E-04	2.86E-07	0.26729	0.00034	3.39547	0.00094	8.836	0.012	0.26719	0.00034	3.39582	0.00096	3.45637	8.831	0.012	**8.771**	**0.012**
92	Okhotnichya	SOP-20-P1	0.78	3.38	1223	1.42E-03	1.90E-06	1.75157	0.00232	1.59552	0.00386	377	7	1.75245	0.00239	1.59622	0.00389	2.73152	377	7	**377**	**7**
93	Okhotnichya	SOP-20-V	0.96	0.76	5863	2.57E-04	3.39E-07	1.53988	0.00202	1.38834	0.00386	>550	n/a	1.53999	0.00202	1.38843	0.00386		>550	n/a	**>550**	**n/a**
94	Okhotnichya	SOP-20-X	0.41	0.45	3035	3.59E-04	6.05E-07	1.12390	0.00147	1.08340	0.00386	>550	n/a	1.12393	0.00148	1.08343	0.00386		>550	n/a	**>550**	**n/a**
95	Okhotnichya	SOP-20-AB	0.47	0.32	4600	2.24E-04	2.93E-07	1.07660	0.00140	1.04926	0.00094	>550	n/a	1.07662	0.00140	1.04927	0.00095		>550	n/a	**>550**	**n/a**

Supplementary Table 1, page 3.

Nu.	Cave	Sample	^{238}U (ppm)	^{232}Th (ppb)	(^{230}Th/^{232}Th)	(^{232}Th/^{238}U)	2σ abs	(^{230}Th/^{238}U)	2σ abs	(^{234}U/^{238}U)	2σ abs	Raw Age (ka before 2010 A.D.)	2σ	(^{230}Th/^{238}U) corr.	2σ abs	(^{234}U/^{238}U) corr.	2σ abs	(^{234}U/^{238}U) initial*	Age corr. (ka before 2010 A.D.)	2σ	**Age (ka before 1950 A.D.)**	**2σ**
96	Okhotnichya	SOP-25-B	2.17	1.03	356	1.56E-04	6.11E-07	0.05476	0.00021	2.16279	0.00236	2.783	0.011	0.05464	0.00022	2.16293	0.00236	2.17210	2.777	0.012	**2.717**	**0.012**
97	Okhotnichya	SOP-25-J	2.56	2.61	3839	3.34E-04	3.75E-06	1.26834	0.00447	1.76969	0.00156	120.96	0.74	1.26841	0.00447	1.76990	0.00156	2.08364	120.94	0.74	**120.88**	**0.74**
98	Okhotnichya	SOP-30-A1.2	0.88	1.61	1675	5.99E-04	1.74E-05	1.01000	0.00289	0.99783	0.00450	>550	n/a	1.01000	0.00290	0.99783	0.00450		>550	n/a	**>550**	**n/a**
99	Okhotnichya	SOP-32-B**	1.17	17.67	297	4.95E-03	1.43E-04	1.47219	0.00422	2.53198	0.00450	85.40	0.41	1.47413	0.00447	2.53827	0.00561	2.95737	85.25	0.45	**85.19**	**0.45**
100	Okhotnichya	SOP-32-K	3.14	0.78	20292	8.15E-05	8.22E-06	1.82337	0.00961	2.41648	0.00336	126.96	1.16	1.82342	0.00961	2.41658	0.00336	3.02805	126.96	1.16	**126.90**	**1.16**
101	Okhotnichya	SOP-32-M	2.66	12.44	1197	1.53E-03	1.54E-04	1.83320	0.00966	2.44272	0.00336	125.70	1.14	1.83426	0.00969	2.44454	0.00350	3.06044	125.65	1.14	**125.59**	**1.14**
102	Shar-Khana	MSHK-4-B	13.30	12.76	3185	3.14E-04	8.43E-07	1.00899	0.00264	1.00466	0.00226	>550	n/a	1.00899	0.00264	1.00466	0.00226		>550	n/a	**>550**	**n/a**
103	Shar-Khana	MSHK-4-E	2.25	6.66	1039	9.67E-04	1.75E-06	1.00788	0.00172	1.00281	0.00226	>550	n/a	1.00789	0.00173	1.00282	0.00227		>550	n/a	**>550**	**n/a**
104	Shar-Khana	MSHK-4-F	2.25	4.97	1367	7.25E-04	1.32E-06	0.99642	0.00172	1.00009	0.00226	>550	n/a	0.99642	0.00173	1.00009	0.00227		>550	n/a	**>550**	**n/a**
105	Shar-Khana	MSHK-7-A	13.89	25.79	1645	6.08E-04	1.42E-06	1.00271	0.00226	1.01726	0.00226	423	20	1.00271	0.00226	1.01727	0.00226	1.05699	423	20	**422**	**20**
106	Shar-Khana	MSHK-7-F	4.03	0.50	23535	4.09E-05	7.18E-08	0.99617	0.00164	1.00926	0.00226	447	25	0.99617	0.00165	1.00926	0.00226	1.03274	447	25	**447**	**25**
107	Shar-Khana	MSHK-16-D1	0.26	1.90	459	2.37E-03	4.10E-06	1.08897	0.00177	1.04852	0.00226	>550	n/a	1.08915	0.00184	1.04861	0.00232		>550	n/a	**>550**	**n/a**
108	Gurvan-Zerd	MGZ-8-F (II)	3.36	0.88	11488	8.60E-05	1.53E-07	1.01451	0.00170	1.00884	0.00226	>550	n/a	1.01451	0.00170	1.00884	0.00226		>550	n/a	**>550**	**n/a**
109	Gurvan-Zerd	MGZ-9-A2 (II)	3.25	0.35	27265	3.47E-05	5.15E-08	1.00402	0.00150	1.00224	0.00098	>550	n/a	1.00402	0.00150	1.00224	0.00098		>550	n/a	**>550**	**n/a**
110	Gurvan-Zerd	MGZ-14-F (II)	2.99	0.22	38448	2.42E-05	4.24E-08	0.99804	0.00164	1.00202	0.00226	>550	n/a	0.99804	0.00164	1.00202	0.00226		>550	n/a	**>550**	**n/a**
111	Lovon-Chombo	MLCH-5-B	1.95	1.53	3879	2.57E-04	4.45E-07	1.00168	0.00163	0.99928	0.00226	>550	n/a	1.00168	0.00163	0.99928	0.00226		>550	n/a	**>550**	**n/a**

Supplementary Table 1: Dating results, isotopic activity ratios are shown in brackets.

(*) Initial ^{234}U/^{238}U activity ratios are presented for the ages younger than 450 ka;

(**) In samples SLL9-2-A+B and SOP-32-B each age is a mix of two different growth periods (in SLL9-2-A+B the layer A contaminated with older layer B; in SOP-32-B the layer B contaminated with material from younger layer A). Because of contamination the dating results of these two layers are not included in Figures 2 and 3.

Supplementary Table 2:									
Name	Unmodelled age (BP)				Modelled age (BP)			Indices A model 93.2 A overall 93.2	
	from	to	depth (cm)	%	from	to	%	A	C
Phase									
Sequence									
Phase									
P_Sequence(1.5)									
Boundary start2			3.80		9712	8351	95.4		98.4
C_Date SB-p6929-bot	8486	8381	3.50	95.4	8484	8377	95.4	99	99.8
C_Date SB-p6929-top	750	740	0.20	95.4	750	740	95.4	98.3	99.5
Boundary =end			0.00		755	-212	95.4		98.8
P_Sequence(1.5)									
Boundary start			7.00		9999	9769	95.4		99
C_Date SB-p7497(1)-I	9943	9805	6.90	95.4	9932	9787	95.4	93.4	99.6
C_Date SB-p7497(1)-A1	464	457	0.10	95.4	464	457	95.4	97.4	98.8
Boundary =end			0.00		469	144	95.4		96.2
P_Sequence(1.5)									
Boundary =start			6.00		9999	9769	95.4		99
C_Date SOP-20-M	8796	8747	5.40	95.4	8796	8746	95.4	98.5	100
C_Date SOP-20-K	7361	7263	4.75	95.4	7360	7262	95.4	99.6	100
C_Date SOP-20-J1	6684	6595	4.30	95.4	6685	6594	95.4	99.6	100
C_Date SOP-20-H	5935	5854	3.70	95.4	5935	5854	95.4	99.4	100
C_Date SOP-20-E2	5290	5240	3.30	95.4	5290	5240	95.4	98.5	100
C_Date SOP-20-E1	4911	4866	2.65	95.4	4912	4865	95.4	98.3	100
C_Date SOP-20-D3.2	4654	4610	2.30	95.4	4654	4610	95.4	98.1	100
C_Date SOP-20-D3.1	3843	3804	1.95	95.4	3843	3803	95.4	97.7	100
C_Date SOP-20-D2.2	3275	3198	1.65	95.4	3275	3198	95.4	99.4	100
C_Date SOP-20-D2.1	2224	2173	1.35	95.4	2225	2172	95.4	98.8	100
C_Date SOP-20-D1	1780	1636	1.05	95.4	1780	1635	95.4	99.7	100
C_Date SOP-20-C	1318	1248	0.75	95.4	1318	1247	95.4	99.3	100
C_Date SOP-20-B	1008	954	0.45	95.4	1009	953	95.4	98.8	100
C_Date SOP-20-A	554	520	0.20	95.4	556	520	95.4	96.8	99.7
Boundary =end			0.00		566	-141	95.4		97.8

Supplementary Tables 2-3: OxCal-4.1 modelling results, the unmodelled and modelled ages are given in years BP. The agreement indices (A) for each age model and for individual events are >60%. Convergence tests (C) are >95%, indicating that the modelled results are a realistic representation of the input data and model (*20*).

Supplementary Table 3:

Name	Unmodelled age (BP)				Modelled age (BP)			Indices A model 86.8 A overall 87.7	
	from	to	depth (cm)	%	from	to	%	A	C
Phase									
Sequence									
Phase									
P_Sequence(1.5)									
Boundary start			7.90		128678	127318	95.4		98.9
C_Date SB-p6919-c4	128540	127471	7.80	95.4	128453	127360	95.4	95.5	99.3
C_Date SB-p6919-C1	119098	118123	2.50	95.4	119262	118336	95.4	86	99.3
Boundary end			2.20		119243	118129	95.4		97
P_Sequence(1.5)									
Boundary start2			11.70		125320	121190	95.4		97.8
C_Date SB-p7497-O	123982	121441	11.30	95.4	123959	121314	95.4	97.6	99.3
C_Date SB-p7497-J	119868	117786	7.20	95.4	119443	118209	95.4	123.2	98.5
Boundary =end			7.00		119243	118129	95.4		97
P_Sequence(1.5)									
Boundary =start			5.50		128678	127318	95.4		98.9
C_Date SOP-2-F3	126759	125323	5.20	95.4	126905	125480	95.4	96.3	99.8
C_Date SOP-2-F1	124905	123482	3.40	95.4	124698	123312	95.4	92.8	99.9
C_Date SOP-2-Ebot	123740	122322	3.10	95.4	123861	122450	95.4	95.8	99.9
C_Date SOP-2-Etop	120109	118768	1.60	95.4	119885	118564	95.4	81.7	97.1
Boundary =end			1.50		119243	118129	95.4		97